On the Performance Gain of Harnessing Non-Line-Of-Sight Propagation for Visible Light-Based Positioning

Bingpeng Zhou, Yuan Zhuang, and Yue Cao

Abstract

Visible light signals undergo non-line-of-sight (NLOS) propagation, and the NLOS links are usually treated as disturbance sources in conventional visible light-based positioning (VLP) methods to simplify signal processing. However, the impact of NLOS propagation on the VLP performance is not fully understood. In this paper, we shall reveal the performance limits of VLP systems under diffuse scattering. First, the closed-form Cramer-Raw lower bounds (CRLBs) on the estimate errors of user detector (UD) location and orientation, respectively, are derived to shed light on the VLP performance limits. Second, the information contribution of NLOS links is quantified to gain insights into the effect of NLOS propagation on the VLP performance. It is shown that VLP can gain additional UD location information from NLOS links via leveraging the NLOS propagation knowledge. In other words, the NLOS channel can be exploited to improve the VLP performance, in addition to the line-of-sight (LOS) channel.

Index Terms

Visible light-based positioning, visible light communication, NLOS effect, localization performance.

I. Introduction

Visible light-based positioning (VLP) is envisioned to be an important technique to improve the performance of indoor localization, with the widespread use of light emitting diodes (LEDs) for illumination. The position and orientation angle of user detector (UD) are critical knowledge for some location-based services such as robotic navigation towards autonomous parcel sorting

This work was supported by Science and Technology Plan of Shenzhen under Grant No. JCYJ20170818114014753.
Bingpeng Zhou is with School of Electronics and Communication Engineering, Sun Yat-Sen University, Guangzhou, China. (email:eebpzhou@sina.com). Yuan Zhuang is with Wuhan University, Wuhan 430079, China. (email:zhy.0908@gmail.com). Yue Cao is with School of Computing and Communications, Lancaster University, U.K. (email:yue.cao@lancaster.ac.uk).

[1], [2] and automatic parking [3]. Hence, VLP has attracted increasing attentions in industry and academia [4]. A number of VLP methods using various measurement signals have been studied, such as the received signal strength (RSS) of visible light [5]–[18] and the combination of RSS with the angle of arrival [19]. A detailed survey of VLP methods is given in [20].

A. Research Motivation

In practice, visible light signals undergo non-line-of-sight (NLOS) propagation, and there are two strategies to handle the NLOS propagation for VLP. The first is called "NLOS-based VLP method". In addition to the line-of-sight (LOS) channel, the NLOS channel is exploited by this method for hopefully extracting more UD location knowledge. Unfortunately, it is established in [26] that the NLOS channel gain is dependent on unknown reflection coefficients and scatterer locations, in addition to the unknown UD location. This will extend the uncertainty set of the VLP problem and hence would degrade the VLP performance. Thus, it is theoretically unclear whether it is helpful for the VLP system to exploit NLOS links and how much performance could be gained from harnessing the NLOS links if it is really helpful. Hence, it is desired to establish the performance limits of the NLOS-based VLP method. The second is called "LOS-based VLP method", for instance, [5]–[18], which treats the complex NLOS links as disturbance sources without any information contribution to the VLP. Since the uncertain parameters of the NLOS channel will complicate VLP algorithm design, only the LOS channel is exploited by this method to simplify its signal processing. This LOS-based VLP solution is simple. Yet, its performance is usually limited, especially in a high SNR environment, in which case the NLOS propagation will become a principal error source [21]. Hence, it is non-trivial to establish the effect of the NLOS propagation on the LOS-based VLP performance.

A number of research works on the performance analysis of VLP methods are already proposed, e.g., [21]–[25]. In [23], the Cramer-Rao lower bound (CRLB) is studied for visible light-based distance estimate, where the LEDs are assumed to radiate downward. Similarly, in [24], the CRLB on the ranging error with a known UD hight is derived. In addition to RSS, the performance limit of time-of-arrival-based VLP is studied in [22] and [25]. However, the required assumptions in the above results restrict their application for general cases. In addition, the above works only focus on the LOS-based UD localization error. Hence, the effect of the NLOS propagation on the VLP performance is unknown. In [21], the performance limits of the

LOS-based VLP method under LOS and/or NLOS propagation are studied. The phenomenon of the unknown NLOS link-caused VLP error floor in high SNR environments is studied using numerical results. However, the associated closed-form analysis is not provided in [21]. In addition, the performance limits of the NLOS-based VLP method are fully unknown, and the performance gain from handling the NLOS propagation is not understood yet. A geometry-based stochastic channel modeling for visible light communications is established in [26], which can be employed to quantitatively analyze the effect of the NLOS propagation on the VLP performance.

B. Contributions Of This Paper

In this paper, we aim to establish the error performance limits of RSS-based VLP methods under NLOS propagation. Specifically, we aim to answering the following open questions:

- Can the NLOS links contribute to the VLP performance?
- If so, how much performance can be gained from harnessing the NLOS links, and how do the NLOS propagation and system parameters (e.g., transmission distance, SNR and the number of LEDs) affect the VLP performance?
- What is the overall performance limit of RSS-based VLP systems under NLOS propagation?

These questions will be answered via the closed-form Fisher information matrix (FIM) analysis, which is challenging due to the complex NLOS modeling. To address this challenge, we shall extract the structured information in the UD location model. The contributions of this paper are summarized as follows.

- *Performance Analysis Of LOS-Based VLP:* We establish the performance limit of the LOS-based VLP method in NLOS propagation environments. Unlike [22]–[25], we obtain the closed-form CRLBs on the UD location and orientation estimate errors, and the effect of the NLOS propagation on the LOS-based VLP performance is also revealed. It is shown that the LOS-based VLP error is affected by the measurement noise and the unknown NLOS links-caused measurement bias. As a result, as the SNR increases, the LOS-based VLP performance will hit an error floor caused by the unknown NLOS links. It should be clarified that, unlike [21], this paper quantitatively analyzes the LOS-based VLP performance limit with closed-form results, and the NLOS propagation-caused VLP error floor of the LOS-based VLP method in high SNR region is quantified for the first time.

- *Performance Analysis Of NLOS-Based VLP:* We conduct the closed-form performance limit analysis of the NLOS-based VLP method. It should be clarified that, unlike [21] which only investigates the LOS-based VLP method, this paper also studies the NLOS-based VLP method which exploits both LOS and NLOS channels. It is shown that the NLOS-based VLP performance is totally affected by the measurement noises. Hence, unlike the LOS-based VLP, the NLOS-based VLP has no error floor. Particularly, the information contribution of the NLOS-based VLP method from the NLOS channel is quantified for the first time in this paper. In addition, the effect of system parameters on the NLOS-based VLP performance is also revealed via asymptotic performance limit analysis.
- *Performance Gain Of Harnessing NLOS Links:* We obtain the closed-form performance gain of the NLOS-based VLP method (from harnessing the NLOS links) over the LOS-based VLP method. It is shown that the NLOS-based VLP performance gain consists of the information gain from the NLOS channel and the NLOS link-caused information loss in the LOS-based VLP. Our performance analysis result implies that harnessing NLOS links can significantly improve the VLP performance, particularly in a high SNR environment.

The rest of this paper is organized as follows. Section II presents the system model. CRLBs are derived in Section III. Performance gain is analysed in Section IV. Asymptotic analysis is given in Section V. Numerical results are given in Section VI. Section VII concludes the paper.

II. System Model

A. System Setup

We consider a VLP system with M LED transmitters and one UD with photodiodes, as illustrated in Fig. 1. Each LED transmitter is equipped with M_E emitters[1] with diverse orientation angles and different locations within a small area of the LED, where $M_E \geq 1$. Let $\mathbf{p}_{k,m} \in \mathbb{R}^3$ and $\mathbf{v}_{k,m} \in \mathbb{R}^3$ be the known location and the orientation vector, respectively, of the kth emitter of the mth LED,[2] for $k = 1 : M_E$ and $m = 1 : M$. These emitters will act as anchors for the UD localization. Let $\mathbf{x} \in \mathbb{R}^3$ and $\mathbf{u} \in \mathbb{R}^3$ be the unknown UD position and orientation vector,

[1]LED array with multiple emitters will be widely adopted in visible light communications for high-rate data transmission [36], [37], [38], [40]. Hence, LED array will be a common practice and can be easily achieved in VLP. The case of single emitter can be covered by our model when M_E reduces to one.

[2]In the following, we use "the (k, m)th emitter" to refer to as "the kth emitter of the mth LED transmitter", for brevity.

respectively. We assume $\|\mathbf{u}\|_2 = 1$ without loss of generality, where $\| \bullet \|_2$ is the ℓ_2-norm on a vector. Let θ_{FOV} and ϕ_{FOV} be the FOVs of UD and the (k, m)th LED emitter, respectively.

B. Diffuse-Scattering Model

We consider a diffuse-scattering model with single-bounce reflection as the signal power of multiple-bounce reflections is very small [26]. We assume that there are $L + 1$ paths between each LED emitter and the UD ($l = 0$ for the LOS paths and $l = 1, \cdots, L$ for NLOS paths). Each single-bounce NLOS link corresponds to one scatterer,[3] as shown in Fig. 2. In addition, we assume the M_E emitters of the same LED are close enough in locations such that they share the same scatterer set.[4] This emitter array will provide diverse location information for alleviating the uncertainties of the NLOS channel. Let $\mathbf{s}_{l,m} \in \mathbb{R}^3$, for $l = 1 : L$, be the unknown scatterer location at the lth path from the mth LED.

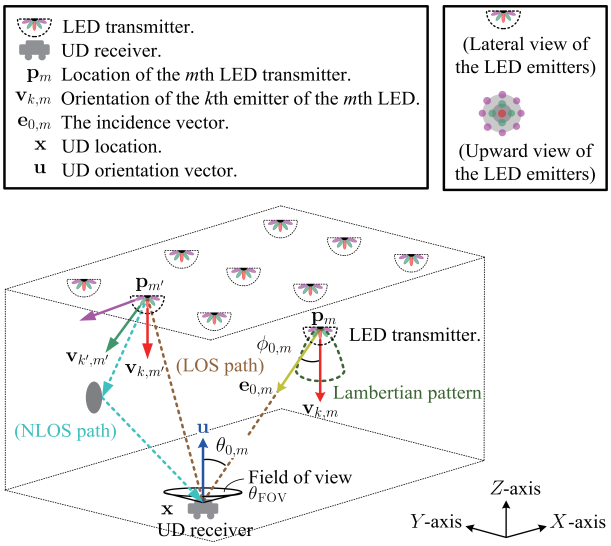

Fig. 1. Illustration of the VLP system.

Visible light RSS depends on the propagation parameters between UD and LEDs. Let $\mathbf{e}_{0,k,m} \in \mathbb{R}^3$ be the irradiation vector of the LOS path from the (k, m)th LED to the UD, and let $\mathbf{e}_{l,k,m} \in \mathbb{R}^3$ be the irradiation vector of the NLOS path from the (k, m)th LED emitter to the scatterer $\mathbf{s}_{l,m}$, respectively, given by $\mathbf{e}_{0,k,m} = \dfrac{\mathbf{x} - \mathbf{p}_{k,m}}{\|\mathbf{x} - \mathbf{p}_{k,m}\|_2}$ and $\mathbf{e}_{l,k,m} = \dfrac{\mathbf{s}_{l,m} - \mathbf{p}_{k,m}}{\|\mathbf{s}_{l,m} - \mathbf{p}_{k,m}\|_2}$, for $l = 1 : L$.

It is worth nothing that, for the LOS link, the irradiation vector $\mathbf{e}_{0,k,m}$ is identical to the incidence vector of the UD. In addition, let $\rho_{0,k,m}$ be the transmission distance of the LOS path associated with the (k, m)th LED emitter, and let $\rho_{l,k,m}$ be the transmission distance associated with the lth path of the (k, m)th LED emitter, for $l = 1 : L$, namely, $\rho_{0,k,m} = \|\mathbf{x} - \mathbf{p}_{k,m}\|_2$,

[3]We consider a discrete reflection model to make a good balance between the model complexity and efficiency, since a continuous model is computationally prohibitive [39]–[41]. Reflection from a continuous surface can be treated as the limiting case of our model when $L \to \infty$. Despite the number of reflections will be infinite, its power is limited and the reflection coefficient is finite, leading to a well-posed VLP problem. Hence, our analysis holds for this limiting case.

[4]This is reasonable since the small difference of emitter locations means a similar geometry of emitters with scatterers and the UD, and hence means their similar reflection paths [42]–[48]. The case of different scatterers for emitters can be viewed as a special case of our model, where those emitters associated with different scatterers are treated as different LEDs.

$\rho_{l,k,m} = \|\mathbf{x}-\mathbf{s}_{l,m}\|_2+\|\mathbf{p}_{k,m}-\mathbf{s}_{l,m}\|_2$. Let $\phi_{0,k,m}$ be the angle between the (k,m)th LED emitter's orientation vector $\mathbf{v}_{k,m}$ and the irradiance vector $\mathbf{e}_{0,k,m}$, i.e., the LOS-path irradiance angle of the (k,m)th LED emitter, as shown in Fig. 2.

Let $\mathbf{e}'_{l,m} \in \mathbb{R}^3$ be the reflection vector of the NLOS path from the scatterer $\mathbf{s}_{l,m}$ to the UD,[5] given by $\mathbf{e}'_{l,m} = \dfrac{\mathbf{x}-\mathbf{s}_{l,m}}{\|\mathbf{x}-\mathbf{s}_{l,m}\|_2}$, for $l = 1:L$. Let $\phi_{l,k,m}$ be the angle between the (k,m)th LED emitter's orientation vector $\mathbf{v}_{k,m}$ and the irradiance vector $\mathbf{e}_{l,k,m}$, i.e., the lth NLOS-path irradiance angle of the (k,m)th LED emitter. Let $\theta_{0,k,m}$ be the LOS-path incidence angle between the UD orientation vector $\mathbf{u}$ and the incidence vector $\mathbf{e}_{0,k,m}$, and let $\theta'_{l,m}$, $l = 1:L$, be the lth NLOS-path incidence angle between the UD orientation vector $\mathbf{u}$ and the reflection vector $\mathbf{e}'_{l,m}$. In a summary, we have $\phi_{l,k,m} = \arccos\left(\mathbf{e}_{l,k,m}^{\top}\mathbf{v}_{k,m}\right)$, for $l = 0:L$, $\theta_{0,k,m} = \arccos\left(-(\mathbf{e}_{0,k,m})^{\top}\mathbf{u}\right)$, and $\theta'_{l,m} = \arccos\left(-(\mathbf{e}'_{l,m})^{\top}\mathbf{u}\right)$, for $l = 1:L$, where $\bullet^{\top}$ denotes the transpose. For the (k,m)th LED emitter, the UD receiver will be able to detect the LOS signal from this LED emitter if UD is within the FOV angle ϕ_{FOV} of this LED emitter and the LOS-path incidence angle $\theta_{0,k,m}$ is within the FOV angle θ_{FOV} of UD, *i.e.*, $\left|\frac{\phi_{0,k,m}}{\phi_{\text{FOV}}}\right| \leq 1$ and $\left|\frac{\theta_{0,k,m}}{\theta_{\text{FOV}}}\right| \leq 1$, where $|\bullet|$ denotes absolute value. Let Ω_R be the set of active LED transmitters, given by $\Omega_R = \left\{m \middle| \left|\frac{\phi_{0,k,m}}{\phi_{\text{FOV}}}\right| \leq 1 \;\&\; \left|\frac{\theta_{0,k,m}}{\theta_{\text{FOV}}}\right| \leq 1,\, k = 1,\cdots,M_E\right\}$. Let $\mathbf{s} \in \mathbb{R}^{3L|\Omega_R|} = \text{vec}[\mathbf{s}_{l,m}|\forall l = 1:L,\, \forall m \in \Omega_R]$, where $\text{vec}[\bullet]$ yields a vector by stacking all elements.

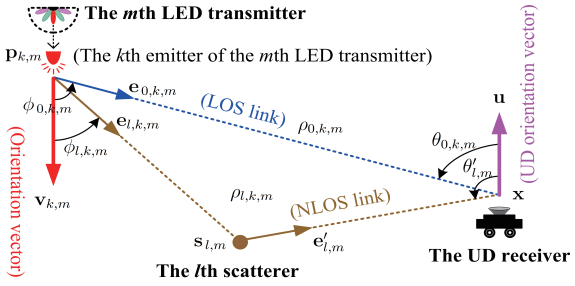

Fig. 2. Illustration of the diffuse scattering scenario.

C. Visible Light RSS Model

The visible light RSS is fundamentally determined by the transmitter steering gain and the receiver response gain as well as the reflection coefficients (for NLOS links).

1) Steering Gain of LED Emitter: The LED emitter steering gain depends on the emitting power and irradiation angle. We assume all LED emitters have the same emission-power W_T. The radiation of LED emitters is usually described by a Lambertian pattern [27] characterized by a Lambertian order $r = -\dfrac{\ln 2}{\ln\cos(A_{\frac{1}{2}})}$, where $A_{\frac{1}{2}}$ is the semi-angle at half power of LED

[5]The index k is omitted in $\mathbf{e}'_{l,m}$ for brevity, since we have assumed that the emitters of the same LED share the same scatterer set and thus the reflection vectors (from the scatterer to the UD) of different emitters are the same.

emitters [28]. Then, for the lth path associated with the irradiance angle $\phi_{l,k,m}$, the steering gain of the (k,m)th LED emitter is given by $W_T(r+1)(\cos(\phi_{l,k,m}))^r$ for the unit emission power.

2) Response Gain of UD: The UD receiver response gain depends on the incidence angle and the transmission distance. For the photodiode of UD, we assume its aperture, optical filter gain and optical concentrator gain are Φ_R, G_R and Γ_R, respectively, where $\Gamma_R = \frac{\zeta_R^2}{(\sin(\theta_{\rm FOV}))^2}$ in which ζ_R is the refractive index of UD optical concentrator and $\theta_{\rm FOV}$ is the UD's FOV [5] shown in Fig. 1. Hence, the UD response gain associated with the lth incidence angle $\theta'_{l,m}$ and the (k,m)th emitter is given by $\frac{\Gamma_R G_R \Phi_R \cos(\theta'_{l,m})}{2\pi\rho^2_{l,k,m}}$, for $l = 1:L$.

3) RSS Model: Based on the above scattering model, the visible light RSS of each path is determined by both the LED steering gain and the UD response gain. Hence, the visible light RSS sample $\mathrm{z}_{k,m}$ associated with the (k,m)th LED emitter is given by [26]

$$\mathrm{z}_{k,m} = \mathrm{h}_{k,m}(\mathbf{x},\mathbf{u},\mathbf{s}) + \epsilon_{k,m},\ \forall k = 1{:}M_E,\ \forall m \in \Omega_R, \tag{1}$$

where $\epsilon_{k,m}$ is the measurement noise, $\mathrm{h}_{k,m}(\mathbf{x},\mathbf{u},\mathbf{s}) = \sum_{l=0:L} \mathrm{h}_{l,k,m}$ is the measurement function, $\mathrm{h}_{l,k,m}$ is the RSS in the lth NLOS path, given by $\mathrm{h}_{0,k,m} = \Psi_R \frac{(r+1)\,(\cos(\phi_{0,k,m}))^r \cos(\theta_{0,k,m})}{\|\mathbf{x}-\mathbf{p}_{k,m}\|_2^2}$ and $\mathrm{h}_{l,k,m} = \Psi_R \wp_{l,m} \eta_k(\mathbf{s}_{l,m}) \frac{\cos(\theta_{l,m})}{\|\mathbf{x}-\mathbf{s}_{l,m}\|_2^2}$, $l = 1:L$, respectively, for $k = 1:M_E$ and $m \in \Omega_R$ [26], [29], [39]. In addition, $\wp_{l,m} \in [0,1)$ is the reflection coefficient of the lth scatterer associated with the (k,m)th LED emitter, which is an unknown scalar, Ψ_R is a known constant dependent on the aperture, optical filter gain and optical concentrator gain of the UD receiver, given by $\Psi_R = \frac{W_T \Gamma_R G_R \Phi_R}{2\pi}$, and $\eta_k(\mathbf{s}_{l,m}) \in \mathbb{R}$ is the (unknown) response gain associated with the transmission distance from the (k,m)th LED emitter to the lth scatterer, given by $\eta_k(\mathbf{s}_{l,m}) = \frac{(r+1)^2(\cos(\phi_{l,k,m}))^r}{2\pi\|\mathbf{p}_{k,m}-\mathbf{s}_{l,m}\|_2^2}$, for $l = 1:L$, which depends on the unknown scatterer location $\mathbf{s}_{l,m}$ but independent of $\mathbf{x}$ and $\mathbf{u}$. For ease of notation, let $\boldsymbol{\wp} \in \mathbb{R}^{L|\Omega_R|} = \mathsf{vec}[\wp_{l,m}|\forall l = 1:L,\ \forall m \in \Omega_R]$, let $\boldsymbol{\beta}_{\rm UD} \in \mathbb{R}^6 = [\mathbf{x};\mathbf{u}]$, let $\boldsymbol{\beta}_{\rm S} \in \mathbb{R}^{4L|\Omega_R|} = [\mathbf{s};\boldsymbol{\wp}]$ and let $\boldsymbol{\alpha} \in \mathbb{R}^{4L|\Omega_R|+6} = [\boldsymbol{\beta}_{\rm UD};\boldsymbol{\beta}_{\rm S}]$, As per the relationship between $\{\theta_{l,m},\phi_{l,m}|\forall l = 0:L\}$ and $\{\mathbf{x},\mathbf{u},\mathbf{s}\}$, $\mathrm{z}_{k,m}$ is rewritten as

$$\mathrm{z}_{k,m} = (\mathbf{g}^{\mathsf{los}}_{k,m}(\mathbf{x}) + \mathbf{g}^{\mathsf{nlos}}_{k,m}(\mathbf{x},\mathbf{s},\boldsymbol{\wp}))^\top \boldsymbol{\mu}(\mathbf{u}) + \epsilon_{k,m},\ \forall k = 1{:}M_E,\ \forall m \in \Omega_R, \tag{2}$$

where $\boldsymbol{\mu}(\mathbf{u}) = \dfrac{\mathbf{u}}{\|\mathbf{u}\|_2}$, $\mathbf{g}^{\mathsf{los}}_{k,m}(\mathbf{x})$ and $\mathbf{g}^{\mathsf{nlos}}_{k,m}(\mathbf{x},\mathbf{s},\wp)$ (both in $\mathbb{R}^3$) are the coefficient vectors of $\boldsymbol{\mu}(\mathbf{u})$ associated with LOS link and NLOS links, respectively, given by [39]

$$\mathbf{g}^{\mathsf{los}}_{k,m}(\mathbf{x}) = \Psi_R \frac{(r+1)\left((\mathbf{x}-\mathbf{p}_{k,m})^\top \mathbf{v}_{k,m}\right)^r}{\|\mathbf{x}-\mathbf{p}_{k,m}\|_2^{r+3}}(\mathbf{p}_{k,m}-\mathbf{x}), \tag{3}$$

$$\mathbf{g}^{\mathsf{nlos}}_{k,m}(\mathbf{x},\mathbf{s},\wp) = \Psi_R \sum_{l=1:L} \wp_{l,m} \frac{(r+1)^2\left((\mathbf{p}_{k,m}-\mathbf{s}_{l,m})^\top \mathbf{v}_{k,m}\right)^r}{2\pi\|\mathbf{p}_{k,m}-\mathbf{s}_{l,m}\|_2^{r+2}\|\mathbf{x}-\mathbf{s}_{l,m}\|_2^3}(\mathbf{s}_{l,m}-\mathbf{x}). \tag{4}$$

To facilitate the analysis, we assume the measurement noise $\epsilon_{k,m}$ in (2) is zero-mean Gaussian, i.e., $\epsilon_{k,m} \sim \mathcal{N}(\epsilon_{k,m}|0,\omega)$, $\forall k = 1:M_E$, $\forall m \in \Omega_R$, with precision ω (inverse variance). Let $\mathbf{z} \in \mathbb{R}^{M_E|\Omega_R|} = \mathsf{vec}[\mathrm{z}_{k,m}|\forall k = 1:M_E, \forall m \in \Omega_R]$. Then, $\mathbf{z} = \mathbf{G}(\mathbf{x},\mathbf{s},\wp)\,\boldsymbol{\mu}(\mathbf{u}) + \boldsymbol{\epsilon}$, where $\boldsymbol{\epsilon} \in \mathbb{R}^{M_E|\Omega_R|}$ is the noise vector, and $\mathbf{G}(\mathbf{x},\mathbf{s},\wp) \in \mathbb{R}^{M_E|\Omega_R|\times 3}$ is given by

$$\mathbf{G} = \mathrm{mat}\Big[(\mathbf{g}^{\mathsf{los}}_{k,m} + \mathbf{g}^{\mathsf{nlos}}_{k,m})^\top | \forall k = 1:M_E, \forall m \in \Omega_R\Big], \tag{5}$$

where $\mathrm{mat}[\bullet]$ yields a matrix by stacking all given row vectors. Let $\mathbf{G}_{\mathsf{los}}$ and $\mathbf{G}_{\mathsf{nlos}} \in \mathbb{R}^{M_E|\Omega_R|\times 3}$ be the coefficient matrices associated with the LOS and the NLOS channels, respectively,

$$\mathbf{G}_{\mathsf{los}} = \mathrm{mat}[(\mathbf{g}^{\mathsf{los}}_{k,m}(\mathbf{x}))^\top | \forall k = 1{:}M_E, \forall m \in \Omega_R], \tag{6}$$

$$\mathbf{G}_{\mathsf{nlos}} = \mathrm{mat}[(\mathbf{g}^{\mathsf{nlos}}_{k,m}(\mathbf{x},\mathbf{s},\wp))^\top | \forall k = 1{:}M_E, \forall m \in \Omega_R]. \tag{7}$$

D. Problem Formulation of VLP

VLP is to estimate the UD location parameters $(\mathbf{x},\mathbf{u})$ from $\{\mathrm{z}_{k,m}|\forall k = 1:M_E,\ \forall m \in \Omega_R\}$, in diffuse scattering environments with unknown parameters $\{\mathbf{s}_{l,m}|\forall l = 1:L,\ \forall m \in \Omega_R\}$ and $\{\wp_{l,m}|\forall l = 1:L,\ \forall m \in \Omega_R\}$. There are two typical methods to solve this VLP problem, based on different assumptions. The first is the LOS-based VLP method, in which only the LOS channel is exploited and the NLOS channel is assumed to be unknown, formulated by

$$\mathcal{P}_{\mathsf{LOS\text{-}VLP}} : (\hat{\mathbf{x}}_{\mathsf{los}}, \hat{\mathbf{u}}_{\mathsf{los}}) = \arg\min_{\mathbf{x},\mathbf{u}} \|\mathbf{z} - \mathbf{G}_{\mathsf{los}}(\mathbf{x})\boldsymbol{\mu}(\mathbf{u})\|_2^2. \tag{8}$$

The second is the NLOS-based VLP exploiting both LOS and NLOS channels, formulated as

$$\mathcal{P}_{\mathsf{NLOS\text{-}VLP}} : (\hat{\mathbf{x}}_{\mathsf{nlos}}, \hat{\mathbf{u}}_{\mathsf{nlos}}) = \arg\min_{\mathbf{x},\mathbf{u}} \underbrace{\min\{\|\mathbf{z} - \mathbf{G}(\mathbf{x},\boldsymbol{\beta}_{\mathrm{S}})\boldsymbol{\mu}(\mathbf{u})\|_2^2 : \forall \boldsymbol{\beta}_{\mathrm{S}}\}}_{\text{Cost function } \vartheta(\mathbf{x},\mathbf{u})}, \tag{9}$$

where it should be noted that our cost function is $\vartheta(\mathbf{x},\mathbf{u})$ which only depends on the UD location parameters $(\mathbf{x},\mathbf{u})$ but independent of $\boldsymbol{\beta}_{\mathrm{S}}$, since $\vartheta(\mathbf{x},\mathbf{u})$ has been minimized over $\boldsymbol{\beta}_{\mathrm{S}}$.

Our goal is to reveal the performance of the above two VLP methods, i.e., $\mathbb{E}\{\|\hat{\mathbf{x}}_{\mathsf{los}}-\mathbf{x}\|_2^2\}$, $\mathbb{E}\{\|\hat{\mathbf{u}}_{\mathsf{los}}-\mathbf{u}\|_2^2\}$, $\mathbb{E}\{\|\hat{\mathbf{x}}_{\mathsf{nlos}}-\mathbf{x}\|_2^2\}$ and $\mathbb{E}\{\|\hat{\mathbf{u}}_{\mathsf{nlos}}-\mathbf{u}\|_2^2\}$, and we also aim to establish the impact of the NLOS propagation on the VLP performance, where $\mathbb{E}\{\bullet\}$ is the expectation over $\mathbf{z}$.

Challenge: However, it is challenging to analyse the LOS- and NLOS-based VLP error performance limits, since there is no closed-form expression of the mean squared VLP errors (e.g., $\mathbb{E}\{\|\hat{\mathbf{x}}_{\mathsf{los}}-\mathbf{x}\|_2^2\}$) due to the nonlinear system function with respect to (w.r.t.) ($\mathbf{x}$, $\mathbf{u}$). □

To address this challenge, we use the inverse matrix lemma [30], [31] for complex FIM functions and the first-order Taylor expansion for nonlinear system models to gain a closed-form CRLB analysis for the VLP error performance.

III. Performance Limits Of VLP

To achieve our goal, we first establish the closed-form CRLBs for the UD location estimates $(\hat{\mathbf{x}},\hat{\mathbf{u}})$ of the typical VLP methods $\mathcal{P}_{\mathsf{LOS\text{-}VLP}}$ and $\mathcal{P}_{\mathsf{NLOS\text{-}VLP}}$, in turn.

A. LOS-Based VLP Performance

We consider the LOS-based VLP method $\mathcal{P}_{\mathsf{LOS\text{-}VLP}}$, where only LOS link is exploited. Let $\upsilon_{\mathbf{x}}$ and $\upsilon_{\mathbf{u}}$ be the unknown-NLOS-link-caused estimate bias of $\hat{\mathbf{x}}_{\mathsf{los}}$ and $\hat{\mathbf{u}}_{\mathsf{los}}$, respectively, given by $\upsilon_{\mathbf{x}}=\|\mathbb{E}\{\hat{\mathbf{x}}_{\mathsf{los}}\}-\mathbf{x}\|_2$, $\upsilon_{\mathbf{u}}=\|\mathbb{E}\{\hat{\mathbf{u}}_{\mathsf{los}}\}-\mathbf{u}\|_2$. In addition, let $\mathfrak{B}_{\mathbf{x}}^{\mathsf{los}}(\mathbf{x},\mathbf{u})$ and $\mathfrak{B}_{\mathbf{u}}^{\mathsf{los}}(\mathbf{x},\mathbf{u})\in\mathbb{S}^3$ denote the CRLBs on the covariance of $\hat{\mathbf{x}}_{\mathsf{los}}$ and $\hat{\mathbf{u}}_{\mathsf{los}}$, respectively.

Theorem 1 (LOS-Based Error Bound): The LOS-based UD location and orientation estimate errors will be bounded as $\mathbb{E}\{\|\hat{\mathbf{x}}_{\mathsf{los}}-\mathbf{x}\|_2^2\}\geq \mathrm{trace}(\mathfrak{B}_{\mathbf{x}}^{\mathsf{los}}(\mathbf{x},\mathbf{u}))+\upsilon_{\mathbf{x}}^2$ and $\mathbb{E}\{\|\hat{\mathbf{u}}_{\mathsf{los}}-\mathbf{u}\|_2^2\}\geq \mathrm{trace}(\mathfrak{B}_{\mathbf{u}}^{\mathsf{los}}(\mathbf{x},\mathbf{u}))+\upsilon_{\mathbf{u}}^2$,, respectively, where $\mathrm{trace}(\bullet)$ is the matrix trace, and

$$\mathfrak{B}_{\mathbf{x}}^{\mathsf{los}}=\Big(\omega\mathbf{H}_{\mathsf{los}}(\mathbf{x})\mathbf{U}(\mathbf{u})\mathbf{F}_{\mathsf{los}}(\mathbf{x})\mathbf{U}^{\top}(\mathbf{u})\,\mathbf{H}_{\mathsf{los}}^{\top}(\mathbf{x})\Big)^{-1}, \tag{10}$$

$$\mathfrak{B}_{\mathbf{u}}^{\mathsf{los}}=\Big(\omega\boldsymbol{\mathcal{R}}(\mathbf{u})\mathbf{G}_{\mathsf{los}}^{\top}(\mathbf{x})\mathbf{V}_{\mathsf{los}}(\mathbf{x},\mathbf{u})\mathbf{G}_{\mathsf{los}}(\mathbf{x})\boldsymbol{\mathcal{R}}^{\top}(\mathbf{u})\Big)^{-1}, \tag{11}$$

where $\mathbf{H}_{\mathsf{los}}(\mathbf{x})\in\mathbb{R}^{3\times 3M_E|\Omega_R|}$, $\boldsymbol{\mathcal{R}}(\mathbf{u})\in\mathbb{S}^3$, $\mathbf{F}_{\mathsf{los}}(\mathbf{x})\in\mathbb{S}^{M_E|\Omega_R|}$ and $\mathbf{U}(\mathbf{u})\in\mathbb{R}^{3M_E|\Omega_R|\times M_E|\Omega_R|}$ are

$$\mathbf{H}_{\mathsf{los}}(\mathbf{x})=[\mathbf{H}_{0,k,m}|\forall k=1:M_E,\forall m\in\Omega_R], \tag{12}$$

$$\mathbf{U}(\mathbf{u})=\mathbf{I}_{M_E|\Omega_R|}\otimes\boldsymbol{\mu}(\mathbf{u}), \tag{13}$$

$$\mathbf{F}_{\mathsf{los}} = \mathbf{I}_{M_E|\Omega_R|} - \mathbf{G}_{\mathsf{los}}(\mathbf{x})\Big(\mathbf{G}_{\mathsf{los}}^{\top}(\mathbf{x})\mathbf{G}_{\mathsf{los}}(\mathbf{x})\Big)^{-1}\mathbf{G}_{\mathsf{los}}^{\top}(\mathbf{x}), \tag{14}$$

$$\boldsymbol{\mathcal{R}}(\mathbf{u}) = \frac{\|\mathbf{u}\|_2^2\,\mathbf{I}_3 - \mathbf{u}\mathbf{u}^{\top}}{\|\mathbf{u}\|_2^3}, \tag{15}$$

in which $\mathbf{I}_3$ is the 3-dimensional identity matrix, $\otimes$ is the Kronecker product, and $\mathbf{H}_{0,k,m} \in \mathbb{R}^{3\times 3}$, $\mathbf{V}_{\mathsf{los}}(\mathbf{x},\mathbf{u}) \in \mathbb{S}^{M_E|\Omega_R|}$ are given by (16) and (17), respectively.

$$\begin{aligned}\mathbf{H}_{0,k,m} = & -\Psi_R\,\rho_{0,k,m}^{-3}(r+1)(\mathbf{e}_{0,k,m}^{\top}\mathbf{v}_{k,m})^{r}\mathbf{I}_3 - \Psi_R\,\rho_{0,k,m}^{-3}r(r+1)(\mathbf{e}_{0,k,m}^{\top}\mathbf{v}_{k,m})^{r-1}\mathbf{v}_{k,m}\mathbf{e}_{0,k,m}^{\top} \\ & + \Psi_R\,\rho_{0,k,m}^{-3}(r+3)(r+1)(\mathbf{e}_{0,k,m}^{\top}\mathbf{v}_{k,m})^{r}\mathbf{e}_{0,k,m}\mathbf{e}_{0,k,m}^{\top},\end{aligned} \tag{16}$$

$$\mathbf{V}_{\mathsf{los}}(\mathbf{x},\mathbf{u}) = \mathbf{I}_{M_E|\Omega_R|} - \mathbf{U}^{\top}(\mathbf{u})\mathbf{H}_{\mathsf{los}}^{\top}(\mathbf{x})\Big(\mathbf{H}_{\mathsf{los}}(\mathbf{x})\mathbf{U}(\mathbf{u})\mathbf{U}^{\top}(\mathbf{u})\mathbf{H}_{\mathsf{los}}^{\top}(\mathbf{x})\Big)^{-1}\mathbf{H}_{\mathsf{los}}(\mathbf{x})\mathbf{U}(\mathbf{u}). \tag{17}$$

Proof: See the proof in APPENDIX A. ■

In [21], a CRLB is also obtained, which considers the LOS environment and the UD location estimate. Unlike [21], we consider the NLOS prorogation, the unknown UD orientation and its effect on the UD location estimate performance, thus leading to a tighter location CRLB $\mathfrak{B}_{\mathbf{x}}^{\mathsf{los}}$. In addition, the closed-form UD orientation CRLB $\mathfrak{B}_{\mathbf{u}}^{\mathsf{los}}$ is obtained in this paper. It is difficult to derive an exact closed-form expression for the LOS-based estimate bias $\upsilon_{\mathbf{x}}$ and $\upsilon_{\mathbf{u}}$, due to the nonlinear system model (2). In the following, we shall approximately characterize the NLOS-link-caused estimate bias $\upsilon_{\mathbf{x}}$ and $\upsilon_{\mathbf{u}}$.

For convenience, let $\boldsymbol{\varsigma}_{\mathsf{nlos}} = \mathbf{G}_{\mathsf{nlos}}(\mathbf{x})\boldsymbol{\mu}(\mathbf{u})$ be the unknown NLOS component of the LOS-based VLP method, let $\boldsymbol{\varsigma}_{\mathsf{bias}}$ be its measurement bias due to $\boldsymbol{\varsigma}_{\mathsf{nlos}}$, and let $\boldsymbol{\varsigma}_{\mathsf{resi}}$ be its residual measurement error (all in $\mathbb{R}^{M_E|\Omega_R|}$), which is given by $\boldsymbol{\varsigma}_{\mathsf{resi}} = \mathbf{z} - \mathbf{G}_{\mathsf{los}}(\hat{\mathbf{x}}_{\mathsf{los}})\boldsymbol{\mu}(\hat{\mathbf{u}}_{\mathsf{los}})$, where $\hat{\mathbf{x}}_{\mathsf{los}}$ is given in $\mathcal{P}_{\mathsf{LOS\text{-}VLP}}$, and $\mathbf{G}_{\mathsf{los}}(\hat{\mathbf{x}}_{\mathsf{los}})\boldsymbol{\mu}(\hat{\mathbf{u}}_{\mathsf{los}})$ is its measurement estimation. We know from system model that $\mathbf{z} = \mathbf{G}_{\mathsf{los}}(\mathbf{x})\boldsymbol{\mu}(\mathbf{u}) + \boldsymbol{\varsigma}_{\mathsf{nlos}} + \boldsymbol{\epsilon} = \mathbf{G}_{\mathsf{los}}(\hat{\mathbf{x}}_{\mathsf{los}})\boldsymbol{\mu}(\hat{\mathbf{u}}_{\mathsf{los}}) + \boldsymbol{\varsigma}_{\mathsf{resi}}$. We can observe that there is a measurement bias in the LOS-based VLP method, i.e., $\mathbf{G}_{\mathsf{los}}(\hat{\mathbf{x}}_{\mathsf{los}})\boldsymbol{\mu}(\hat{\mathbf{u}}_{\mathsf{los}}) - \mathbf{G}_{\mathsf{los}}(\mathbf{x})\boldsymbol{\mu}(\mathbf{u})$, denoted by $\boldsymbol{\varsigma}_{\mathsf{bias}} \in \mathbb{R}^{M_E|\Omega_R|}$, with $\boldsymbol{\varsigma}_{\mathsf{bias}} = \boldsymbol{\varsigma}_{\mathsf{nlos}} - \boldsymbol{\varsigma}_{\mathsf{resi}}$, where $\mathbf{G}_{\mathsf{los}}(\mathbf{x})\boldsymbol{\mu}(\mathbf{u})$ stands for the true measurement without noises. We can also observe that $\boldsymbol{\varsigma}_{\mathsf{bias}}$ mainly stems from $\boldsymbol{\varsigma}_{\mathsf{nlos}}$ and $\boldsymbol{\varsigma}_{\mathsf{resi}}$ since we have assumed the measurement noise $\boldsymbol{\epsilon}$ is zero-mean. In the following, we will show that the NLOS-caused UD location estimation bias $\upsilon_{\mathbf{x}}$ and $\upsilon_{\mathbf{u}}$ are totally determined by $\boldsymbol{\varsigma}_{\mathsf{bias}}$.

Theorem 2 (LOS-Based VLP Bias): The LOS-based estimation biases $\upsilon_{\mathbf{x}}$ and $\upsilon_{\mathbf{u}}$ are approximately given by $\upsilon_{\mathbf{x}} \approx \|\boldsymbol{\varsigma}_{\mathsf{bias}}\|_2\|\mathbf{H}_{\mathsf{los}}(\mathbf{x})\mathbf{U}(\mathbf{u})\|_2^{-1}$ and $\upsilon_{\mathbf{u}} \approx \|\boldsymbol{\varsigma}_{\mathsf{bias}}\|_2\|\boldsymbol{\mathcal{R}}(\mathbf{u})\mathbf{G}_{\mathsf{los}}^{\top}(\mathbf{x})\|_2^{-1}$, respec-

tively, and the approximation error is a second-order infinitesimal $\mathcal{O}\Big(\|\hat{\mathbf{x}}_{\mathsf{los}}-\mathbf{x}\|_2^2+\|\hat{\mathbf{u}}_{\mathsf{los}}-\mathbf{u}\|_2^2\Big)$ which can be safely ignored.[6]

Proof: See APPENDIX B. ■

We have the following Corollary to establish the scaling rule of LOS-based estimation bias w.r.t. the measurement bias, which sheds lights on the impact of the unknown NLOS component on the LOS-based VLP error performance.

Corollary 1 (Scaling Rule of LOS-Based VLP Bias): The LOS-based location and orientation biases follow $\lim\limits_{\|\boldsymbol{\varsigma}_{\mathsf{bias}}\|_2\to 0}\dfrac{\upsilon_{\mathbf{x}}}{\|\boldsymbol{\varsigma}_{\mathsf{bias}}\|_2}\approx\|\mathbf{H}_{\mathsf{los}}(\mathbf{x})\mathbf{U}(\mathbf{u})\|_2^{-1}$ and $\lim\limits_{\|\boldsymbol{\varsigma}_{\mathsf{bias}}\|_2\to 0}\dfrac{\upsilon_{\mathbf{u}}}{\|\boldsymbol{\varsigma}_{\mathsf{bias}}\|_2}\approx\|\boldsymbol{\mathcal{R}}(\mathbf{u})\mathbf{G}_{\mathsf{los}}^{\top}(\mathbf{x})\|_2^{-1}$, where the second-order approximation error $\mathcal{O}\Big(\|\hat{\mathbf{x}}_{\mathsf{los}}-\mathbf{x}\|_2^2+\|\hat{\mathbf{u}}_{\mathsf{los}}-\mathbf{u}\|_2^2\Big)$ can be safely ignored.

Proof: This Corollary directly follows from Theorem 2. ■

We draw the following Remark on the NLOS effect on the LOS-based VLP performance.

Remark 1: The LOS-based VLP biases reduce with the NLOS signal strength, and the reducing rate depends on the LOS channel gain. For a large localization area, NLOS signals will reduce fast due to the long-distance fading. Hence, the NLOS-caused VLP bias will be alleviated. □

Considering that there is no exact closed-form expression of the LOS-based VLP error, we have the following Theorem to establish an approximate mean squared error (AMSE) for the LOS-based VLP, which helps to gain insights into the overall performance of LOS-based VLP.

Theorem 3 (LOS-based VLP Error): The LOS-based UD location and orientation errors are approximately characterized, respectively, as follows,

$$\mathbb{E}\{\|\hat{\mathbf{x}}_{\mathsf{los}}-\mathbf{x}\|_2^2\}\approx(\|\boldsymbol{\varsigma}_{\mathsf{bias}}\|_2^2+\mathbb{E}\{\|\boldsymbol{\epsilon}\|_2^2\})\|\mathbf{H}_{\mathsf{los}}(\mathbf{x})\mathbf{U}(\mathbf{u})\|_2^{-2}, \tag{18}$$

$$\mathbb{E}\{\|\hat{\mathbf{u}}_{\mathsf{los}}-\mathbf{u}\|_2^2\}\approx(\|\boldsymbol{\varsigma}_{\mathsf{bias}}\|_2^2+\mathbb{E}\{\|\boldsymbol{\epsilon}\|_2^2\})\|\mathbf{G}_{\mathsf{los}}(\mathbf{x})\boldsymbol{\mathcal{R}}^{\top}(\mathbf{u})\|_2^{-2}, \tag{19}$$

with an approximation error of $\mathcal{O}(\|\hat{\mathbf{x}}_{\mathsf{los}}-\mathbf{x}\|_2^2+\|\hat{\mathbf{u}}_{\mathsf{los}}-\mathbf{u}\|_2^2)$ that can be safely ignored.

Proof: See the proof in APPENDIX C. ■

It is shown that the LOS-based VLP error stems from the measurement noise $\boldsymbol{\epsilon}$ and the NLOS link-caused measurement bias $\boldsymbol{\varsigma}_{\mathsf{bias}}$. In the following, we reveal how the LOS-based VLP error is formed and quantified. An illustration of the LOS-based VLP error source using the signal projection onto LOS channel-associated measurement space is presented in Fig. 3,

[6] $f(x)\sim\mathcal{O}(g(x))$ as $x\to\infty$ means there exists a positive number C_1 and a number X_0 such that $|f(x)|\le C_1|g(x)|$ holds for all $x>X_0$.

where $(\mathbf{x}_{\mathsf{true}}, \mathbf{u}_{\mathsf{true}})$ denotes the true value of $(\mathbf{x}, \mathbf{u})$, while $\mathbf{x}_{\mathsf{bias}}$ and $\mathbf{x}_{\mathsf{unb}}$ denote the biased and unbiased error of LOS-based location estimate $\hat{\mathbf{x}}_{\mathsf{los}}$, given by $\mathbf{x}_{\mathsf{unb}} = \hat{\mathbf{x}}_{\mathsf{los}} - \mathbb{E}\{\hat{\mathbf{x}}_{\mathsf{los}}\}$ and $\mathbf{x}_{\mathsf{bias}} = \mathbb{E}\{\hat{\mathbf{x}}_{\mathsf{los}}\} - \mathbf{x}_{\mathsf{true}}$, respectively, and $\mathbf{z}_{\mathsf{true}} = \mathbf{G}_{\mathsf{los}}(\mathbf{x}_{\mathsf{true}})\boldsymbol{\mu}(\mathbf{u}_{\mathsf{true}})$ denotes the true measurement of the LOS channel. We can see that the LOS-based estimate $(\hat{\mathbf{x}}_{\mathsf{los}}, \hat{\mathbf{u}}_{\mathsf{los}})$ corresponds to the sample image $\hat{\mathbf{z}}_{\mathsf{los}} = \mathbf{G}_{\mathsf{los}}(\hat{\mathbf{x}}_{\mathsf{los}})\boldsymbol{\mu}(\hat{\mathbf{u}}_{\mathsf{los}})$ in the range space, which is an orthogonal projection (with the least squared error from $\mathbf{z}$ as formulated in $\mathcal{P}_{\mathsf{LOS\text{-}VLP}}$) of $\mathbf{z}$ onto the LOS channel's range space $\mathbb{Z}_{\mathsf{los}} = \{\mathbf{G}_{\mathsf{los}}(\mathbf{x})\boldsymbol{\mu}(\mathbf{u}) : \forall \mathbf{x}, \forall \mathbf{u}\}$.

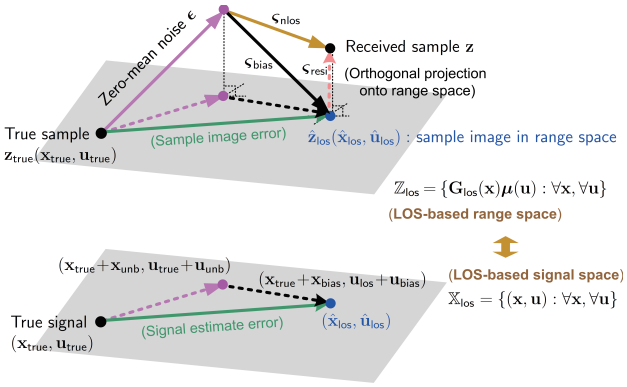

Fig. 3. Illustration of LOS-based VLP error source projection.

Remark 2 (Measurement Error $\mapsto$ LOS-Based Range Error): Firstly, the measurement error $\boldsymbol{\epsilon} + \boldsymbol{\varsigma}_{\mathsf{nlos}}$ will lead to a sample image error $\hat{\mathbf{z}}_{\mathsf{los}} - \mathbf{z}_{\mathsf{true}}$ in the LOS-based range space $\mathbb{Z}_{\mathsf{los}}$. Specifically, the sample image error $\hat{\mathbf{z}}_{\mathsf{los}} - \mathbf{z}_{\mathsf{true}}$ stems from the projection of the zero-mean measurement noise $\boldsymbol{\epsilon}$ and the bias measurement error $\boldsymbol{\varsigma}_{\mathsf{bias}}$, i.e., the projection of $\boldsymbol{\varsigma}_{\mathsf{bias}} + \boldsymbol{\epsilon}$, where $\boldsymbol{\varsigma}_{\mathsf{bias}} = \boldsymbol{\varsigma}_{\mathsf{nlos}} - \boldsymbol{\varsigma}_{\mathsf{resi}}$. Hence, the LOS-based location estimation error $\hat{\mathbf{x}}_{\mathsf{los}} - \mathbf{x}_{\mathsf{true}}$ can be cast as the summation of the unbiased error $\mathbf{x}_{\mathsf{unb}} = \hat{\mathbf{x}}_{\mathsf{los}} - \mathbb{E}\{\hat{\mathbf{x}}_{\mathsf{los}}\}$ and the biased error $\mathbf{x}_{\mathsf{bias}} = \mathbb{E}\{\hat{\mathbf{x}}_{\mathsf{los}}\} - \mathbf{x}_{\mathsf{true}}$, which stems from the projection of the zero-mean measurement error $\boldsymbol{\epsilon}$ and the bias measurement error $\boldsymbol{\varsigma}_{\mathsf{bias}}$, respectively, as shown in Fig. 3 and described in Theorem 3. In addition, since $\boldsymbol{\epsilon}$ is zero-mean, the overall measurement error $\boldsymbol{\varsigma}_{\mathsf{bias}} + \boldsymbol{\epsilon}$ of the LOS channel follows $\mathbb{E}\{\|\boldsymbol{\varsigma}_{\mathsf{bias}} + \boldsymbol{\epsilon}\|_2^2\} = \mathbb{E}\{\|\boldsymbol{\varsigma}_{\mathsf{bias}}\|_2^2\} + \mathbb{E}\{\|\boldsymbol{\epsilon}\|_2^2\}$. □

Remark 3 (LOS-Based Range Error $\mapsto$ LOS-based Estimate Error): Secondly, the LOS-based image error $\hat{\mathbf{z}}_{\mathsf{los}} - \mathbf{z}_{\mathsf{true}}$ leads to the LOS-based VLP error $\|\hat{\mathbf{x}}_{\mathsf{los}} - \mathbf{x}\|_2$. The scaling rate associated with the projection from the LOS-based range space $\mathbb{Z}_{\mathsf{los}}$ to the LOS-based estimator space $\mathbb{X}_{\mathsf{los}} = \{(\mathbf{x}, \mathbf{u}) | \forall \mathbf{x}, \forall \mathbf{u}\}$ is dominated by the first-order Taylor component of the LOS channel function $\mathbf{G}_{\mathsf{los}}(\mathbf{x})\boldsymbol{\mu}(\mathbf{u})$ w.r.t. $(\mathbf{x}, \mathbf{u})$ around $(\mathbf{x}, \mathbf{u}) = (\mathbf{x}_{\mathsf{true}}, \mathbf{u}_{\mathsf{true}})$, i.e., $\nabla_{\mathbf{x}}(\mathbf{G}(\mathbf{x}_{\mathsf{true}})\boldsymbol{\mu}_{\mathsf{true}}) = \mathbf{H}_{\mathsf{los}}(\mathbf{x}_{\mathsf{true}})\mathbf{U}(\mathbf{u}_{\mathsf{true}})$ and $\nabla_{\mathbf{u}}(\mathbf{G}(\mathbf{x}_{\mathsf{true}})\boldsymbol{\mu}_{\mathsf{true}}) = \boldsymbol{\mathcal{R}}(\mathbf{u}_{\mathsf{true}})\mathbf{G}_{\mathsf{los}}^{\top}(\mathbf{x}_{\mathsf{true}})$. Therefore, the projection of measurement error $\mathbb{E}\{\|\boldsymbol{\varsigma}_{\mathsf{bias}}\|_2^2\} + \mathbb{E}\{\|\boldsymbol{\epsilon}\|_2^2\}$ in the range space onto the signal space should be tuned down by this scaling rate, as described in Theorem 3. □

It is implied by Theorem 3 that, as SNR increases, the unknown NLOS component will become the dominant localization error source, and hence the LOS-based VLP performance will

hit an error floor due to the bias from the non-ignorable NLOS links. We have the following Corollary to characterize this error floor of the LOS-based VLP method.

Corollary 2 (NLOS Link-Caused Error Floor in LOS-Based VLP): As the SNR increases infinitely, the LOS-based VLP error will tend to the following asymptotic limit:

$$\lim_{\mathsf{SNR}\to\infty} \mathbb{E}\{\|\hat{\mathbf{x}}_{\mathsf{los}}-\mathbf{x}\|_2^2\} \approx \mathbb{E}\{\|\boldsymbol{\varsigma}_{\mathsf{bias}}\|_2^2\}\|\mathbf{H}_{\mathsf{los}}(\mathbf{x})\mathbf{U}(\mathbf{u})\|_2^{-2}, \tag{20}$$

$$\lim_{\mathsf{SNR}\to\infty} \mathbb{E}\{\|\hat{\mathbf{u}}_{\mathsf{los}}-\mathbf{u}\|_2^2\} \approx \mathbb{E}\{\|\boldsymbol{\varsigma}_{\mathsf{bias}}\|_2^2\}\|\mathbf{G}_{\mathsf{los}}(\mathbf{x})\boldsymbol{\mathcal{R}}^{\top}(\mathbf{u})\|_2^{-2}, \tag{21}$$

with an approximation error of $\mathcal{O}\Big(\|\hat{\mathbf{x}}_{\mathsf{los}}-\mathbf{x}\|_2^2 + \|\hat{\mathbf{u}}_{\mathsf{los}}-\mathbf{u}\|_2^2\Big)$ that can be safely ignored.

Proof: As $\mathsf{SNR}\to\infty$, $\|\boldsymbol{\epsilon}\|_2 \to 0$. Thus, Corollary 2 can be obtained from Theorem 3. ■

This means that the LOS-based VLP error floor in a high SNR region is determined by the NLOS-caused measurement bias $\boldsymbol{\varsigma}_{\mathsf{bias}}$ in RSS measurements. Unlike the LOS-based VLP method, the NLOS-based VLP method harnesses the NLOS links to mitigate the negative effect of diffuse scattering on the achieved VLP performance. We will show that, by exploiting NLOS propagation knowledge, this NLOS-caused VLP error floor will vanish.

B. NLOS-Based VLP Performance

The following Theorem establishes the performance limit of the NLOS-based VLP method $\mathcal{P}_{\mathsf{NLOS\text{-}VLP}}$ that exploits both LOS and NLOS links.

Theorem 4 (NLOS-Based Error Bound): The NLOS-based UD location and orientation estimate errors will be bounded from below, respectively, as follows,

$$\mathbb{E}\{\|\hat{\mathbf{x}}_{\mathsf{nlos}} - \mathbf{x}\|_2^2\} \geq \mathrm{trace}(\boldsymbol{\mathfrak{B}}_{\mathbf{x}}^{\mathsf{nlos}}(\mathbf{x},\mathbf{u};\mathbf{s},\boldsymbol{\wp})), \tag{22}$$

$$\mathbb{E}\{\|\hat{\mathbf{u}}_{\mathsf{nlos}} - \mathbf{u}\|_2^2\} \geq \mathrm{trace}(\boldsymbol{\mathfrak{B}}_{\mathbf{u}}^{\mathsf{nlos}}(\mathbf{x},\mathbf{u};\mathbf{s},\boldsymbol{\wp})), \tag{23}$$

where $\boldsymbol{\mathfrak{B}}_{\mathbf{x}}^{\mathsf{nlos}}(\mathbf{x},\mathbf{u};\mathbf{s},\boldsymbol{\wp})$ and $\boldsymbol{\mathfrak{B}}_{\mathbf{u}}^{\mathsf{nlos}}(\mathbf{x},\mathbf{u};\mathbf{s},\boldsymbol{\wp}) \in \mathbb{S}^3$ denote the NLOS-based location CRLB and orientation CRLB (conditioned on $(\mathbf{s},\boldsymbol{\wp})$), respectively, given by

$$\boldsymbol{\mathfrak{B}}_{\mathbf{x}}^{\mathsf{nlos}} = \Big(\omega\mathbf{H}(\mathbf{x})\mathbf{U}(\mathbf{u})\mathbf{F}(\mathbf{x})\mathbf{U}^{\top}(\mathbf{u})\mathbf{H}^{\top}(\mathbf{x}) - \boldsymbol{\mathcal{L}}_{\mathbf{x}}^{\mathsf{nlos}}(\mathbf{x},\mathbf{u})\Big)^{-1}, \tag{24}$$

$$\boldsymbol{\mathfrak{B}}_{\mathbf{u}}^{\mathsf{nlos}} = \Big(\omega\boldsymbol{\mathcal{R}}(\mathbf{u})\mathbf{G}^{\top}(\mathbf{x})\mathbf{V}(\mathbf{x},\mathbf{u})\mathbf{G}(\mathbf{x})\boldsymbol{\mathcal{R}}^{\top}(\mathbf{u}) - \boldsymbol{\mathcal{L}}_{\mathbf{u}}^{\mathsf{nlos}}(\mathbf{x},\mathbf{u})\Big)^{-1}, \tag{25}$$

where $\boldsymbol{\mathcal{L}}_{\mathbf{x}}^{\mathsf{nlos}}(\mathbf{x},\mathbf{u})$ and $\boldsymbol{\mathcal{L}}_{\mathbf{u}}^{\mathsf{nlos}}(\mathbf{x},\mathbf{u}) \in \mathbb{S}^3$ denote the uncertain NLOS channel state-caused infor-

mation reduction in UD location and orientation, respectively, which are given later.

Proof: See the proof in APPENDIX D. ■

In addition, $\mathbf{F}(\mathbf{x}) \in \mathbb{S}^{M_E|\Omega_R|}$ is given by $\mathbf{F}(\mathbf{x}) = \mathbf{I}_{M_E|\Omega_R|} - \mathbf{G}(\mathbf{x})(\mathbf{G}^\top(\mathbf{x})\mathbf{G}(\mathbf{x}))^{-1}\mathbf{G}^\top(\mathbf{x})$, where $\mathbf{G}(\mathbf{x})$ is given in (5), and $\mathbf{V}(\mathbf{x},\mathbf{u}) \in \mathbb{S}^{M_E|\Omega_R|}$ is given by

$$\mathbf{V}(\mathbf{x},\mathbf{u}) = \mathbf{I}_{M_E|\Omega_R|} - \mathbf{U}^\top(\mathbf{u})\mathbf{H}^\top(\mathbf{x})\Big(\mathbf{H}(\mathbf{x})\mathbf{U}(\mathbf{u})\mathbf{U}^\top(\mathbf{u})\mathbf{H}^\top(\mathbf{x})\Big)^{-1}\mathbf{H}(\mathbf{x})\mathbf{U}(\mathbf{u}). \tag{26}$$

In addition, $\mathbf{H}(\mathbf{x}) \in \mathbb{R}^{3\times 3M_E|\Omega_R|}$ is given by

$$\mathbf{H}(\mathbf{x}) = [\mathbf{H}_{k,m}|\forall k = 1\!:\!M_E, \forall m \in \Omega_R] \;\; \text{with} \;\; \mathbf{H}_{k,m} = \mathbf{H}_{0,k,m} + \sum_{l=1:L} \mathbf{H}_{l,k,m}, \tag{27}$$

where $\mathbf{H}_{0,k,m}$ is given by (16), and $\mathbf{H}_{l,k,m} \in \mathbb{R}^{3\times 3}$, for $l = 1:L$, is given by

$$\mathbf{H}_{l,k,m} = 3\Psi_R \frac{(r+1)^2}{2\pi} \frac{\wp_{l,m}\varphi_{l,k,m}(\mathbf{s}_{l,m})}{\|\mathbf{x}-\mathbf{s}_{l,m}\|_2^5} (\mathbf{x}-\mathbf{s}_{l,m})(\mathbf{x}-\mathbf{s}_{l,m})^\top - \Psi_R \frac{(r+1)^2}{2\pi} \frac{\wp_{l,m}\varphi_{l,k,m}(\mathbf{s}_{l,m})}{\|\mathbf{x}-\mathbf{s}_{l,m}\|_2^3} \mathbf{I}_3,$$

in which $\varphi_{l,k,m}(\mathbf{s}_{l,m}) \in \mathbb{R}$ is given by $\varphi_{l,k,m}(\mathbf{s}_{l,m}) = \dfrac{\big((\mathbf{s}_{l,m}-\mathbf{p}_{k,m})^\top \mathbf{v}_{k,m}\big)^r}{\|\mathbf{s}_{l,m}-\mathbf{p}_{k,m}\|_2^{r+2}}$. In addition, $\boldsymbol{\mathcal{L}}_{\mathbf{x}}^{\mathsf{nlos}}(\mathbf{x},\mathbf{u})$ and $\boldsymbol{\mathcal{L}}_{\mathbf{u}}^{\mathsf{nlos}}(\mathbf{x},\mathbf{u}) \in \mathbb{S}^3$ are given by

$$\boldsymbol{\mathcal{L}}_{\mathbf{x}}^{\mathsf{nlos}} = \boldsymbol{\mathcal{P}}_{\mathbf{x}}\mathbf{W}_{\mathbf{x}}^{-1}\boldsymbol{\mathcal{P}}_{\mathbf{x}}^\top - \omega\mathbf{H}(\mathbf{x})\mathbf{U}(\mathbf{u})\mathbf{F}^\perp(\mathbf{x})\mathbf{U}^\top(\mathbf{u})\mathbf{H}^\top(\mathbf{x}), \tag{28}$$

$$\boldsymbol{\mathcal{L}}_{\mathbf{u}}^{\mathsf{nlos}} = \boldsymbol{\mathcal{P}}_{\mathbf{u}}\mathbf{W}_{\mathbf{u}}^{-1}\boldsymbol{\mathcal{P}}_{\mathbf{u}}^\top - \omega\boldsymbol{\mathcal{R}}(\mathbf{u})\mathbf{G}^\top(\mathbf{x})\mathbf{V}^\perp(\mathbf{x},\mathbf{u})\mathbf{G}(\mathbf{x})\boldsymbol{\mathcal{R}}^\top(\mathbf{u}), \tag{29}$$

where $\boldsymbol{\mathcal{P}}_{\mathbf{x}}$, $\boldsymbol{\mathcal{P}}_{\mathbf{u}} \in \mathbb{R}^{3\times(4L|\Omega_R|+3)}$ and $\mathbf{W}_{\mathbf{x}}$, $\mathbf{W}_{\mathbf{u}} \in \mathbb{S}^{(4L|\Omega_R|+3)}$ are given by (50) and (51), respectively, while $\mathbf{F}^\perp(\mathbf{x})$ and $\mathbf{V}^\perp(\mathbf{x},\mathbf{u}) \in \mathbb{S}^{M_E|\Omega_R|}$ are given by $\mathbf{F}^\perp(\mathbf{x}) = \mathbf{I}_{M_E|\Omega_R|} - \mathbf{F}(\mathbf{x})$, $\mathbf{V}^\perp(\mathbf{x},\mathbf{u}) = \mathbf{I}_{M_E|\Omega_R|} - \mathbf{V}(\mathbf{x},\mathbf{u})$.

Remark 4 (Vanished Error Floor in NLOS-Based VLP): It should be noted that the information reduction $\boldsymbol{\mathcal{L}}_{\mathbf{x}}^{\mathsf{nlos}}$ and $\boldsymbol{\mathcal{L}}_{\mathbf{u}}^{\mathsf{nlos}}$ are proportional to ω. Therefore, when $\mathsf{SNR} \to \infty$, the NLOS-based VLP error bound $\mathfrak{B}_{\mathbf{x}}^{\mathsf{nlos}}$ and $\mathfrak{B}_{\mathbf{u}}^{\mathsf{nlos}}$ will approach zero, thanks to the exploitation of the NLOS propagation knowledge in the UD localization, as implied by Theorem 4. Hence, there is no error floor in the VLP method after exploiting the NLOS propagation knowledge, as SNR increases. This implies a huge localization performance gain from harnessing NLOS links. □

In the following, we shall quantify the achieved performance gain of the NLOS-based VLP method (from exploiting the NLOS links) over the LOS-based VLP method.

IV. Gain from Harnessing the NLOS Links

Let us start with the analysis of the LOS-based VLP information sources, following which we will elaborate the NLOS-based VLP information sources to establish the performance gain from harnessing NLOS propagation. An illustration of the LOS-based and NLOS-based VLP information sources is provided in Fig. 4.

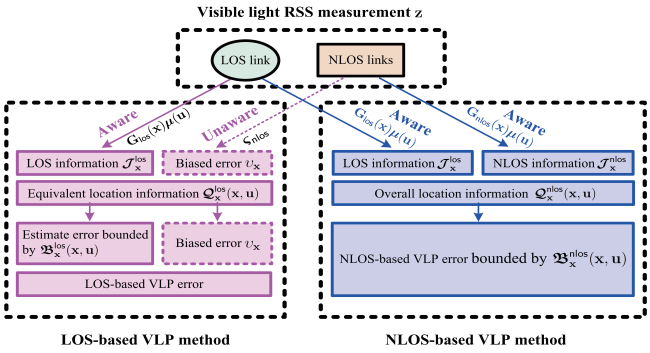

Fig. 4. Illustration of VLP information sources.

A. Information Formation of LOS-Based VLP

For convenience, we define several information notations for the LOS-based VLP method.

- *(LOS Link-Contributed FIM):* Let $\boldsymbol{\mathcal{J}}_{\mathbf{x}}^{\mathsf{los}}(\mathbf{x},\mathbf{u}) \in \mathbb{S}^3$ be the UD location information from the LOS link, i.e., the inverse of LOS-based CRLB $\boldsymbol{\mathfrak{B}}_{\mathbf{x}}^{\mathsf{los}}(\mathbf{x},\mathbf{u})$, given by

$$\boldsymbol{\mathcal{J}}_{\mathbf{x}}^{\mathsf{los}} = \omega \mathbf{H}_{\mathsf{los}}(\mathbf{x})\mathbf{U}(\mathbf{u})\mathbf{F}_{\mathsf{los}}(\mathbf{x})\mathbf{U}^{\top}(\mathbf{u})\,\mathbf{H}_{\mathsf{los}}^{\top}(\mathbf{x}), \tag{30}$$

  where $\mathbf{F}_{\mathsf{los}}(\mathbf{x})$ is given by (14). This FIM quantifies the theoretically maximum information of the LOS-based VLP method from the LOS channel of a clean environment without diffuse scattering (i.e., $\varsigma_{\mathsf{bias}} = 0$).
- *(Equivalent FIM of LOS-Based VLP):* Let $\tilde{\boldsymbol{\mathcal{Q}}}_{\mathbf{x}}^{\mathsf{los}}(\mathbf{x},\mathbf{u}) \in \mathbb{S}^3$ denote the equivalent location FIM (i.e., the accuracy) of the LOS-based VLP method, which is defined as the inverse of the associated error coverable matrix, i.e.,

$$\tilde{\boldsymbol{\mathcal{Q}}}_{\mathbf{x}}^{\mathsf{los}}(\mathbf{x},\mathbf{u}) = \left(\tilde{\boldsymbol{\mathfrak{B}}}_{\mathbf{x}}^{\mathsf{los}}(\mathbf{x},\mathbf{u})\right)^{-1}, \tag{31}$$

  where $\tilde{\boldsymbol{\mathfrak{B}}}_{\mathbf{x}}^{\mathsf{los}}(\mathbf{x},\mathbf{u}) \in \mathbb{S}^3$ is the covariance of the LOS-based UD location error, i.e.,

$$\tilde{\boldsymbol{\mathfrak{B}}}_{\mathbf{x}}^{\mathsf{los}}(\mathbf{x},\mathbf{u}) = \mathbb{E}\{(\hat{\mathbf{x}}_{\mathsf{los}} - \mathbf{x})(\hat{\mathbf{x}}_{\mathsf{los}} - \mathbf{x})^{\top}\}. \tag{32}$$

  This FIM quantifies the actual net-information gained (from the LOS channel) by the LOS-based VLP method in a diffuse-scattering environment.

- *(Measurement Bias-Caused Equivalent Location FIM):* Let $\boldsymbol{\mathcal{J}}_{\mathbf{x}}^{\mathsf{bias}}(\mathbf{x},\mathbf{u}) \in \mathbb{S}^3$ denote the equivalent location FIM associated with the LOS-based location estimate bias, given by

$$\boldsymbol{\mathcal{J}}_{\mathbf{x}}^{\mathsf{bias}} = \|\boldsymbol{\varsigma}_{\mathsf{bias}}\|_2^{-2}\mathbf{H}_{\mathsf{los}}(\mathbf{x})\mathbf{U}(\mathbf{u})\mathbf{U}^{\top}(\mathbf{u})\,\mathbf{H}_{\mathsf{los}}^{\top}(\mathbf{x}). \tag{33}$$

This FIM stands for a "virtual" information associated with the unknown NLOS links.

Then, we have the following lemma to establish $\tilde{\boldsymbol{\mathcal{Q}}}_{\mathbf{x}}^{\mathsf{los}}(\mathbf{x},\mathbf{u})$ for the LOS-based VLP method.

Lemma 1 (LOS-Based VLP's Equivalent FIM): The equivalent information matrix of the LOS-based VLP method is approximately given by

$$\tilde{\boldsymbol{\mathcal{Q}}}_{\mathbf{x}}^{\mathsf{los}}(\mathbf{x},\mathbf{u}) \approx \underbrace{\Big(\big(\boldsymbol{\mathcal{J}}_{\mathbf{x}}^{\mathsf{los}}(\mathbf{x},\mathbf{u})\big)^{-1} + \big(\boldsymbol{\mathcal{J}}_{\mathbf{x}}^{\mathsf{bias}}(\mathbf{x},\mathbf{u})\big)^{-1}\Big)^{-1}}_{\boldsymbol{\mathcal{Q}}_{\mathbf{x}}^{\mathsf{los}}(\mathbf{x},\mathbf{u})}, \tag{34}$$

with an approximation error of $\mathcal{O}\Big(\|\hat{\mathbf{x}}_{\mathsf{los}}-\mathbf{x}\|_2^2 + \|\hat{\mathbf{u}}_{\mathsf{los}}-\mathbf{u}\|_2^2\Big)$, where $\boldsymbol{\mathcal{J}}_{\mathbf{x}}^{\mathsf{los}}$ and $\boldsymbol{\mathcal{J}}_{\mathbf{x}}^{\mathsf{bias}}$ is given by (30) and (33), respectively.

Proof: See the proof in APPENDIX E. ■

Combining (31), (32) and lemma 1, we know the LOS-based UD location estimate error follows $\mathbb{E}\Big\{(\hat{\mathbf{x}}_{\mathsf{los}}-\mathbf{x})(\hat{\mathbf{x}}_{\mathsf{los}}-\mathbf{x})^{\top}\Big\} \approx \Big(\boldsymbol{\mathcal{J}}_{\mathbf{x}}^{\mathsf{los}}(\mathbf{x},\mathbf{u})\Big)^{-1} + \Big(\boldsymbol{\mathcal{J}}_{\mathbf{x}}^{\mathsf{bias}}(\mathbf{x},\mathbf{u})\Big)^{-1}$, which is consistent with Theorem 3. In addition, the LOS link-contributed information $\boldsymbol{\mathcal{J}}_{\mathbf{x}}^{\mathsf{los}}$ is affected by the measurement accuracy ω as shown in (30), whereas the bias information $\boldsymbol{\mathcal{J}}_{\mathbf{x}}^{\mathsf{bias}}$ is determined by the inverse measurement bias strength $\|\boldsymbol{\varsigma}_{\mathsf{bias}}\|_2^{-2}$ as shown in (33). Hence, the LOS-based location estimate error stems from both the measurement noise $\boldsymbol{\epsilon}$ and the measurement bias $\boldsymbol{\varsigma}_{\mathsf{bias}}$ (including the unaware NLOS components $\boldsymbol{\varsigma}_{\mathsf{nlos}}$), as described in (34) and Theorem 3.

The equivalent information $\boldsymbol{\mathcal{Q}}_{\mathbf{x}}^{\mathsf{los}}(\mathbf{x},\mathbf{u})$ describes the LOS-based UD localization accuracy performance limit, i.e., the overall net information under NLOS propagation. It is implied in (34) that the NLOS prorogation will lead to an information reduction and hence performance loss in the LOS-based VLP method, i.e., $\boldsymbol{\mathcal{Q}}_{\mathbf{x}}^{\mathsf{los}} \preceq \boldsymbol{\mathcal{J}}_{\mathbf{x}}^{\mathsf{los}}(\mathbf{x},\mathbf{u})$. Let $\boldsymbol{\mathcal{W}}_{\mathbf{x}}^{\mathsf{los}} \in \mathbb{S}^3 = \boldsymbol{\mathcal{J}}_{\mathbf{x}}^{\mathsf{los}} - \boldsymbol{\mathcal{Q}}_{\mathbf{x}}^{\mathsf{los}}$ be such NLOS-caused information reduction.

Corollary 3 (Closed-Form Information Reduction in LOS-Based VLP): For the LOS-based VLP method, the information reduction due to the unknown NLOS links is given by

$$\boldsymbol{\mathcal{W}}_{\mathbf{x}}^{\mathsf{los}}(\mathbf{x},\mathbf{u}) = \Big((\boldsymbol{\mathcal{J}}_{\mathbf{x}}^{\mathsf{los}})^{-1}\boldsymbol{\mathcal{J}}_{\mathbf{x}}^{\mathsf{bias}}(\boldsymbol{\mathcal{J}}_{\mathbf{x}}^{\mathsf{los}})^{-1} + (\boldsymbol{\mathcal{J}}_{\mathbf{x}}^{\mathsf{los}})^{-1}\Big)^{-1}, \tag{35}$$

where $\boldsymbol{\mathcal{J}}_{\mathbf{x}}^{\mathsf{los}}$ and $\boldsymbol{\mathcal{J}}_{\mathbf{x}}^{\mathsf{bias}}$ is given by (30) and (33), respectively.

Proof: We have $\boldsymbol{\mathcal{W}}_{\mathbf{x}}^{\mathsf{los}} = \boldsymbol{\mathcal{J}}_{\mathbf{x}}^{\mathsf{los}} - \boldsymbol{\mathcal{Q}}_{\mathbf{x}}^{\mathsf{los}} = \boldsymbol{\mathcal{J}}_{\mathbf{x}}^{\mathsf{los}} - \left((\boldsymbol{\mathcal{J}}_{\mathbf{x}}^{\mathsf{los}})^{-1} + (\boldsymbol{\mathcal{J}}_{\mathbf{x}}^{\mathsf{bias}})^{-1}\right)^{-1}$. Then, applying for the inverse matrix lemma [30], [31], we arrive at (35). Thus, Corollary 3 is proved. ■

Remark 5 (NLOS-Caused Performance Loss in LOS-Based VLP): We can see from (35) that the information reduction matrix $\boldsymbol{\mathcal{W}}_{\mathbf{x}}^{\mathsf{los}} \succeq \mathbf{0}$, i.e., there must be an information loss in LOS-based VLP due to the NLOS propagation. This is because the unknown NLOS links in RSS measurements behave as disturbance sources for the LOS-based VLP method and hence degrade the achieved VLP performance. Therefore, the LOS-based location information will be diluted by the bias information $\boldsymbol{\mathcal{J}}_{\mathbf{x}}^{\mathsf{bias}}$ from $\boldsymbol{\mathcal{J}}_{\mathbf{x}}^{\mathsf{los}}$ to $\boldsymbol{\mathcal{Q}}_{\mathbf{x}}^{\mathsf{los}}$, in a manner described in (34). This complies with our intuition. Ideally, for a clean environment without diffuse scattering, the LOS-based VLP information will be exactly the LOS channel information $\boldsymbol{\mathcal{J}}_{\mathbf{x}}^{\mathsf{los}}(\mathbf{x}, \mathbf{u})$ without discount. □

B. Information Composition of NLOS-Based VLP

For the NLOS-based VLP method, since the NLOS propagation knowledge is exploited, there will be information gain from NLOS links. Let $\boldsymbol{\mathcal{J}}_{\mathbf{x}}^{\mathsf{nlos}}(\mathbf{x}, \mathbf{u}) \in \mathbb{S}^3$ be the UD location information from the NLOS links (established later). Then, the overall CRLB $\boldsymbol{\mathfrak{B}}_{\mathbf{x}}^{\mathsf{nlos}}(\mathbf{x}, \mathbf{u})$ on the NLOS-based UD location estimate error (in Theorem 4) follows

$$\boldsymbol{\mathfrak{B}}_{\mathbf{x}}^{\mathsf{nlos}}(\mathbf{x}, \mathbf{u}) = \Big(\underbrace{\boldsymbol{\mathcal{J}}_{\mathbf{x}}^{\mathsf{los}}(\mathbf{x}, \mathbf{u}) + \boldsymbol{\mathcal{J}}_{\mathbf{x}}^{\mathsf{nlos}}(\mathbf{x}, \mathbf{u})}_{\boldsymbol{\mathcal{Q}}_{\mathbf{x}}^{\mathsf{nlos}}(\mathbf{x}, \mathbf{u})} \Big)^{-1}, \tag{36}$$

as illustrated in Fig. 4, where $\boldsymbol{\mathcal{Q}}_{\mathbf{x}}^{\mathsf{nlos}}(\mathbf{x}, \mathbf{u}) \in \mathbb{S}^3$ is the overall information of the NLOS-based VLP method, which is from both LOS and NLOS links; and the NLOS links-contributed information $\boldsymbol{\mathcal{J}}_{\mathbf{x}}^{\mathsf{nlos}}(\mathbf{x}, \mathbf{u})$ is given by the following Corollary.

Corollary 4 (Location Information from NLOS Links): In the NLOS-based VLP method, the UD location information associated with the NLOS links is given by

$$\boldsymbol{\mathcal{J}}_{\mathbf{x}}^{\mathsf{nlos}}(\mathbf{x}, \mathbf{u}) = \boldsymbol{\mathcal{D}}_{\mathbf{x}}^{\mathsf{nlos}}(\mathbf{x}, \mathbf{u}) - \boldsymbol{\mathcal{S}}_{\mathbf{x}}^{\mathsf{nlos}}(\mathbf{x}, \mathbf{u}), \tag{37}$$

where $\boldsymbol{\mathcal{D}}_{\mathbf{x}}^{\mathsf{nlos}}(\mathbf{x}, \mathbf{u}) \in \mathbb{S}^3$ is the cross information from LOS and NLOS links, given by $\boldsymbol{\mathcal{D}}_{\mathbf{x}}^{\mathsf{nlos}}(\mathbf{x}, \mathbf{u}) = \omega \mathbf{H}_{\mathsf{nlos}}(\mathbf{x}) \mathbf{U}(\mathbf{u}) \mathbf{U}^{\top}(\mathbf{u}) \mathbf{H}_{\mathsf{los}}^{\top}(\mathbf{x}) + \omega \mathbf{H}_{\mathsf{los}}(\mathbf{x}) \mathbf{U}(\mathbf{u}) \mathbf{U}^{\top}(\mathbf{u}) \mathbf{H}_{\mathsf{nlos}}^{\top}(\mathbf{x}) + \omega \mathbf{H}_{\mathsf{nlos}}(\mathbf{x}) \mathbf{U}(\mathbf{u}) \mathbf{U}^{\top}(\mathbf{u}) \mathbf{H}_{\mathsf{nlos}}^{\top}(\mathbf{x})$,

where $\mathbf{H}_{\mathsf{nlos}}(\mathbf{x}) \in \mathbb{R}^{3\times 3M_E|\Omega_R|}$ is given by

$$\mathbf{H}_{\mathsf{nlos}}(\mathbf{x}) = \Big[\sum_{l=1:L} \mathbf{H}_{l,k,m} | \forall k = 1:M_E, \forall m \in \Omega_R\Big], \tag{38}$$

and $\boldsymbol{\mathcal{S}}_{\mathbf{x}}^{\mathsf{nlos}}(\mathbf{x},\mathbf{u}) \in \mathbb{S}^3 = \boldsymbol{\mathcal{P}}_{\mathbf{x}}\mathbf{W}_{\mathbf{x}}^{-1}\boldsymbol{\mathcal{P}}_{\mathbf{x}}^{\top} - \omega\mathbf{H}_{\mathsf{los}}(\mathbf{x})\mathbf{U}(\mathbf{u})\mathbf{F}_{\mathsf{los}}^{\perp}(\mathbf{x})\mathbf{U}^{\top}(\mathbf{u})\mathbf{H}_{\mathsf{los}}^{\top}(\mathbf{x})$ is the information reduction, in which $\boldsymbol{\mathcal{P}}_{\mathbf{x}}$ and $\mathbf{W}_{\mathbf{x}}$ are given by (50), while $\mathbf{F}_{\mathsf{los}}^{\perp}(\mathbf{x})$ is given by $\mathbf{F}_{\mathsf{los}}^{\perp}(\mathbf{x}) = \mathbf{G}_{\mathsf{los}}(\mathbf{x})(\mathbf{G}_{\mathsf{los}}^{\top}(\mathbf{x})\mathbf{G}_{\mathsf{los}}(\mathbf{x}))^{-1}\mathbf{G}_{\mathsf{los}}^{\top}(\mathbf{x})$.

Proof: See the proof in APPENDIX F. ■

C. Performance Gain

In the following, we establish the performance gain of the NLOS-based VLP method over the LOS-based VLP method. For continence, let the approximate error $\breve{\boldsymbol{\mathcal{B}}}_{\mathbf{x}}^{\mathsf{los}} = (\boldsymbol{\mathcal{Q}}_{\mathbf{x}}^{\mathsf{los}})^{-1}$ (with $\boldsymbol{\mathcal{Q}}_{\mathbf{x}}^{\mathsf{los}}$ given by (34)) sand for the error performance of the LOS-based VLP method.

Compared with the NLOS-based and the LOS-based VLP information formation in (36) and (34), respectively, we can observe that the NLOS links impose a negative effect on the LOS-based VLP (leading to an information reduction $\boldsymbol{\mathcal{W}}_{\mathbf{x}}^{\mathsf{los}}$) while a positive effect on the NLOS-based VLP (leading to an information gain $\boldsymbol{\mathcal{J}}_{\mathbf{x}}^{\mathsf{nlos}}$). Hence, the performance gain of the NLOS-based VLP over the LOS-based VLP includes two parts: the NLOS link-contributed information gain $\boldsymbol{\mathcal{J}}_{\mathbf{x}}^{\mathsf{nlos}}$ and the NLOS link-caused information reduction $\boldsymbol{\mathcal{W}}_{\mathbf{x}}^{\mathsf{los}}$ in the LOS-based VLP method.

Corollary 5 (NLOS-Based VLP Information Gain over LOS-Based VLP): The performance gain of the NLOS-based VLP over the LOS-based VLP is given by

$$\boldsymbol{\mathcal{Q}}_{\mathbf{x}}^{\mathsf{gain}}(\mathbf{x},\mathbf{u}) = \boldsymbol{\mathcal{W}}_{\mathbf{x}}^{\mathsf{los}}(\mathbf{x},\mathbf{u}) + \boldsymbol{\mathcal{J}}_{\mathbf{x}}^{\mathsf{nlos}}(\mathbf{x},\mathbf{u}), \tag{39}$$

where $\boldsymbol{\mathcal{W}}_{\mathbf{x}}^{\mathsf{los}}$ and $\boldsymbol{\mathcal{J}}_{\mathbf{x}}^{\mathsf{nlos}}$ are given by (35) and (37), respectively.

Proof: This Corollary directly follows from the associated definition that $\boldsymbol{\mathcal{Q}}_{\mathbf{x}}^{\mathsf{gain}}(\mathbf{x},\mathbf{u}) = \boldsymbol{\mathcal{Q}}_{\mathbf{x}}^{\mathsf{nlos}}(\mathbf{x},\mathbf{u}) - \boldsymbol{\mathcal{Q}}_{\mathbf{x}}^{\mathsf{los}}(\mathbf{x},\mathbf{u}) = \boldsymbol{\mathcal{J}}_{\mathbf{x}}^{\mathsf{nlos}} + \underbrace{\boldsymbol{\mathcal{J}}_{\mathbf{x}}^{\mathsf{los}} - \Big((\boldsymbol{\mathcal{J}}_{\mathbf{x}}^{\mathsf{los}})^{-1} + (\boldsymbol{\mathcal{J}}_{\mathbf{x}}^{\mathsf{bias}})^{-1}\Big)^{-1}}_{\boldsymbol{\mathcal{W}}_{\mathbf{x}}^{\mathsf{los}}}$. ■

Then, the following Theorem establishes that harnessing the NLOS links will contribute to VLP, if the NLOS-associated information gain $\boldsymbol{\mathcal{J}}_{\mathbf{x}}^{\mathsf{nlos}}$ satisfies a certain condition.

Theorem 5 (NLOS-Based VLP's Performance Gain): The NLOS-based VLP error bound is lower than the LOS-based VLP error, i.e., $\mathfrak{B}_{\mathbf{x}}^{\mathsf{nlos}} \preceq \breve{\boldsymbol{\mathcal{B}}}_{\mathbf{x}}^{\mathsf{los}}$, if $\boldsymbol{\mathcal{Q}}_{\mathbf{x}}^{\mathsf{gain}}(\mathbf{x},\mathbf{u}) \succeq \mathbf{0}_{3\times 3}$ is satisfied.

Proof: It can be easily verified from (39) that if that condition is satisfied, we have $\boldsymbol{\mathcal{Q}}_{\mathbf{x}}^{\mathsf{gain}} \succeq \mathbf{0}_{3\times 3}$. Then, based on (36) and (34) in lemma 1, we finally arrive at $\boldsymbol{\mathfrak{B}}_{\mathbf{x}}^{\mathsf{nlos}} \preceq \breve{\boldsymbol{\mathcal{B}}}_{\mathbf{x}}^{\mathsf{los}}$. ■

It should be noted that the condition $\boldsymbol{\mathcal{Q}}_{\mathbf{x}}^{\mathsf{gain}}(\mathbf{x},\mathbf{u}) \succeq \mathbf{0}_{3\times 3}$ is satisfied almost surely. This is because the NLOS link with a well-defined propagation model indeed has useful UD location information, and meanwhile the unknown NLOS link-caused information reduction in the LOS-based VLP method is non-ignorable, i.e., $\boldsymbol{\mathcal{W}}_{\mathbf{x}}^{\mathsf{los}} \succeq \mathbf{0}$. Hence, it is possible to improve the VLP performance via exploiting UD location knowledge from the NLOS links, given the NLOS propagation model. Yet, this is challenging due to the non-convex nature of NLOS-based VLP, and hence it calls for an efficient algorithm design. For the NLOS-based UD orientation estimate, we have the same conclusion as above, which is omitted for brevity.

V. Asymptotic Performance Analysis

We can see from Theorem 4 that the NLOS-based VLP error is affected by the transmission distance, SNR and the number of visible LED emitters. In this section, we shall reveal the effect of these critical parameters on the performance of the NLOS-based VLP method.

Firstly, we have the following Corollary for the impact of the NLOS-based CRLB w.r.t. SNR.

Corollary 6 (The Effect Of SNR): The NLOS-based VLP error bounds follow $\mathrm{trace}(\boldsymbol{\mathfrak{B}}_{\mathbf{x}}^{\mathsf{nlos}}(\mathbf{x},\mathbf{u})) \sim \Theta(\mathsf{SNR}^{-1})$ and $\mathrm{trace}(\boldsymbol{\mathfrak{B}}_{\mathbf{u}}^{\mathsf{nlos}}(\mathbf{x},\mathbf{u})) \sim \Theta(\mathsf{SNR}^{-1})$, as $\mathsf{SNR} \to \infty$.[7]

Proof: It directly follows from Theorem 4, where it should be noted that $\boldsymbol{\mathcal{L}}_{\mathbf{x}}^{\mathsf{nlos}}(\mathbf{x},\mathbf{u})$ and $\boldsymbol{\mathcal{L}}_{\mathbf{u}}^{\mathsf{nlos}}(\mathbf{x},\mathbf{u})$ are $\Theta(\mathsf{SNR}^{-1})$, which can be easily verified by their closed-form expressions. ■

This Corollary implies that the NLOS-based VLP error is totally affected by measurement noise strength, and it reduces with the SNR. Hence, unlike the LOS-based VLP method, the NLOS-based VLP method will no longer have a NLOS-caused error floor in a high-SNR region due to the harnessing of NLOS links. This complies with Remark 4.

For ease of notation, let $\rho_{\min} = \min\{\rho_{k,l,m} | \forall l = 0:L,\ \forall k = 1:M_E,\ \forall m \in \Omega_R\}$ be the minimum transmission distance between LEDs and the UD.

Secondly, for the scaling rule of the NLOS-based VLP error CRLB w.r.t. the transmission distance between LED and UD, we have the following conclusion.

[7] $f(x) \sim \Theta(g(x))$ as $x \to \infty$ means there exists C_1, $C_2 > 0$ and a constant X_0 such that $C_1|g(x)| \le |f(x)| \le C_2|g(x)|$ holds for all $x > X_0$.

Corollary 7 (The Effect Of Transmission Distance): The NLOS-Based VLP error bounds scale with the transmission distance between LED and UD as follows,[8] as $\rho_{\min} \to \infty$:

$$\mathrm{trace}(\mathfrak{B}_{\mathbf{x}}^{\mathsf{nlos}}(\mathbf{x},\mathbf{u})) \sim \Omega(\rho_{\min}^{6}), \tag{40}$$

$$\mathrm{trace}(\mathfrak{B}_{\mathbf{u}}^{\mathsf{nlos}}(\mathbf{x},\mathbf{u})) \sim \Omega(\rho_{\min}^{4}). \tag{41}$$

Proof: See APPENDIX H. ■

This indicates that the NLOS-based UD location estimate error is increasing with the transmission distance in the sixth power, while the UD orientation estimate error is increasing with the transmission distance in the fourth power. This is fundamentally determined by the physical propagation model of visible light signals. This means that a larger area needs more LEDs to preserve a satisfactory VLP performance.

Thirdly, for the scaling of the NLOS-based VLP error CRLB w.r.t. the number of LEDs, we have the following conclusion.

Corollary 8 (The Effect Of LED Set Size): We assume that the LEDs are uniformly distributed within the room. Then, the NLOS-based error bounds follows $\mathrm{trace}(\mathfrak{B}_{\mathbf{x}}^{\mathsf{nlos}}(\mathbf{x},\mathbf{u})) \sim \Theta(|\Omega_R|^{-1})$, and $\mathrm{trace}(\mathfrak{B}_{\mathbf{u}}^{\mathsf{nlos}}(\mathbf{x},\mathbf{u})) \sim \Theta(|\Omega_R|^{-1})$, respectively, as $|\Omega_R| \to \infty$.

Proof: See APPENDIX I. ■

This means that the NLOS-based VLP error reduces with the number of independent signal sources, at the rate of $\Theta(|\Omega_R|^{-1})$.

Fourthly, for the impact of scatterer reflection coefficients on the NLOS-based and LOS-based VLP performance, respectively, we have the following Corollaries.

Corollary 9 (The Effect Of Reflection Coefficient On NLOS-Based VLP Performance): The NLOS-based VLP error bound $\mathfrak{B}_{\mathbf{x}}^{\mathsf{nlos}}(\mathbf{x},\mathbf{u})$ and $\mathfrak{B}_{\mathbf{u}}^{\mathsf{nlos}}(\mathbf{x},\mathbf{u})$ follows $\mathrm{trace}(\mathfrak{B}_{\mathbf{x}}^{\mathsf{nlos}}(\mathbf{x},\mathbf{u})) \sim \Theta(\|\wp\|_2^{-2})$, and $\mathrm{trace}(\mathfrak{B}_{\mathbf{u}}^{\mathsf{nlos}}(\mathbf{x},\mathbf{u})) \sim \Theta(\|\wp\|_2^{-2})$, respectively, as $\|\wp\|_2 \to \infty$.[9]

Corollary 10 (The Effect Of Reflection Coefficient On LOS-Based VLP Performance): The LOS-based VLP error bounds $\mathfrak{B}_{\mathbf{x}}^{\mathsf{los}}(\mathbf{x},\mathbf{u})$ and $\mathfrak{B}_{\mathbf{u}}^{\mathsf{los}}(\mathbf{x},\mathbf{u})$ follows $\mathrm{trace}(\mathfrak{B}_{\mathbf{x}}^{\mathsf{los}}(\mathbf{x},\mathbf{u})) \sim \Theta(\|\wp\|_2^{2})$,

[8] $f(x) \sim \Omega(g(x))$ as $x \to \infty$ means there exists a positive number C_2 and a number X_0 such that $|f(x)| \geq C_2|g(x)|$ holds for all $x > X_0$.

[9] Despite $\|\wp\|_2 \in (0,1)$ in practice, the following asymptotic limits under $\|\wp\|_2 \to \infty$ are still useful for understanding the scaling rule of the VLP performance as the NLOS signal strength increases. For $\|\wp\|_2 \to 0$, the performance limits of LOS-based VLP can be directly implied by Theorem 2 and 3. In addition, NLOS-based VLP will reduce to LOS-based VLP in such a case, which means identical performance limits of them.

and $\mathrm{trace}(\mathfrak{B}_{\mathbf{u}}^{\mathsf{los}}(\mathbf{x},\mathbf{u})) \sim \Theta(\|\wp\|_2^2)$, respectively, the reflection coefficient strength $\|\wp\|_2 \to \infty$.

Proof: See APPENDIX J. ■

We can observe that, when the reflection coefficient increases, the LOS-based VLP error increases accordingly, while the NLOS-based VLP error reduces, both at a second-order rate, which are totally opposite behaviors. This is because of the different mechanisms for handling the NLOS channel and hence different information structures of these two VLP methods.

The scatterer reflection coefficient will affect the strength of NLOS signals $\|\varsigma_{\mathsf{nlos}}\|_2$, which will further affect the NLOS propagation-caused equivalent information $\mathcal{J}_{\mathbf{x}}^{\mathsf{bias}}(\mathbf{x},\mathbf{u})$ of the LOS-based VLP method (see (33)) and the NLOS channel-contributed information $\mathcal{J}_{\mathbf{x}}^{\mathsf{nlos}}(\mathbf{x},\mathbf{u})$ of the NLOS-based VLP method (see (37)). Yet, $\mathcal{J}_{\mathbf{x}}^{\mathsf{bias}}(\mathbf{x},\mathbf{u})$ leads an effect of information reduction to the LOS-based VLP method (see (34)), while $\mathcal{J}_{\mathbf{x}}^{\mathsf{nlos}}(\mathbf{x},\mathbf{u})$ leads an effect of information increase to the NLOS-based VLP method (see (36)). Hence, the reflection coefficient has an entirely different impact on these two VLP methods. Specifically, for the LOS-based VLP method, a small reflection coefficient leads to a small interference and hence a small NLOS-caused error floor and finally a small VLP error. On the contrary, for the NLOS-based VLP method, a small reflection coefficient leads to a small information contribution from the NLOS channel, thus leading to a large VLP error.

VI. NUMERICAL RESULTS

In this section, simulation results are presented to examine the obtained theoretical results of the LOS- and NLOS-based VLP performance limits.

A. Simulation Settings

We consider $M = 15$ LED transmitters uniformly installed on the ceiling of a room with the size of $9[\mathrm{m}] \times 9[\mathrm{m}] \times 4[\mathrm{m}]$. In addition, we assume there are $M_E = 25$ emitters at each LED transmitter, which are uniformly distributed within a circle area of $1[\mathrm{cm}^2]$ around the LED transmitter centre. The orientation of all LED emitters are assumed to be with downwards direction with an arbitrary azimuth direction and a random polar angle. The UD appears in the room at a random location and with a random orientation. In addition, we assume $\Phi_R = 0.5\,[\mathrm{cm}^2]$, $r = 1$, $G_R = 1$, $\Gamma_R = 2.25$, and $\theta_{\mathrm{FOV}} = \phi_{\mathrm{FOV}} = \pi/2$. These parameter settings follow from a typical LED setup that are widely adopted in papers such as [5], [12], [33], [34]. Furthermore,

we consider the measurement noise strength is 10^{-8} such that the SNR is around 30 [dB], and we set $L = 4$ diffuse paths between each LED emitter and the UD [35], unless specified otherwise. The four scatterers between each LED transmitter and UD are randomly distributed within the room. Moreover, we set $\wp_{l,m}$ in $(0, 0.8)$ at random, for each diffuse link.

We adopt the VLP algorithms in [13] and [17] as the LOS-based and the NLOS-based VLP methods, respectively, which are used to make a comparison between the VLP method-achieved localization performance and our CRLB-based theoretical localization performance.

B. Result Analysis

1) The Effect of SNR: The error performance of the LOS- and NLOS-based VLP methods v.s. SNR is shown in Fig. 5, where the SNR varies from -20 [dB] to 80 [dB] and the measurement noise strength reduces accordingly while the emitting power is fixed. It is shown that the LOS-based VLP error reduces as SNR increases and finally hits an error floor in the high SNR region, due to the unknown NLOS links. This means that the NLOS links will become the dominant error source of the LOS-based VLP method in high SNR conditions, and hence an advanced VLP algorithm to harnessing the NLOS links is desired. In contrast, it is shown in Fig. 5 that the NLOS-based VLP error performance reduces as the SNR increases, due to the exploitation of the NLOS propagation knowledge, as revealed in Theorem 4. In addition, we can see from Fig. 5 that the performance gain of NLOS-based VLP over LOS-based VLP increases with SNR. In the high SNR region, the NLOS interference will become the dominant error source, and hence VLP method will achieve a large performance gain from harnessing the NLOS links. This complies with Corollary 5 and Theorem 5.

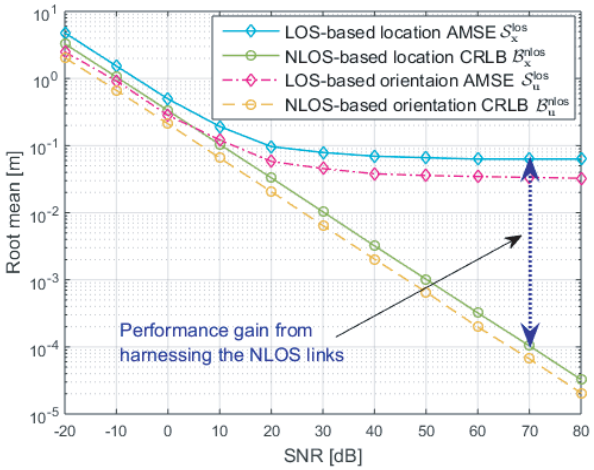

Fig. 5. VLP error performance v.s. SNR.

In addition, we consider two UD paths, shown in Fig. 6, to evaluate the associated NLOS-based VLP performance. We can see from Fig. 7 that the VLP will achieve a better performance when the UD height is lower than 3[m] for a 4[m]-high room, due to the better sight. In addition, the VLP has a larger error when the UD is closer to the wall.

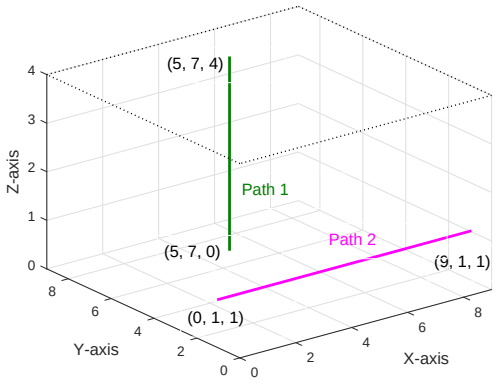

Fig. 6. Illustration of UD paths.

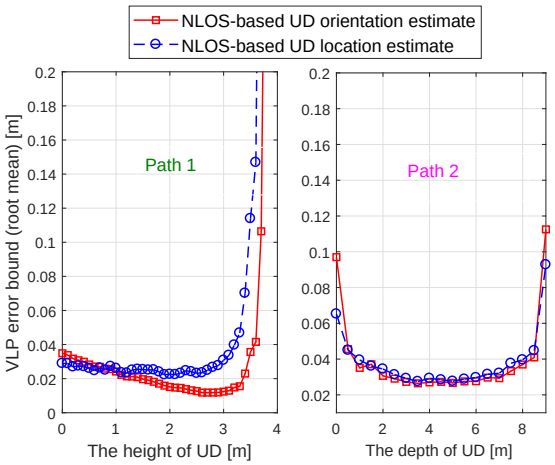

Fig. 7. VLP performance under different UD paths.

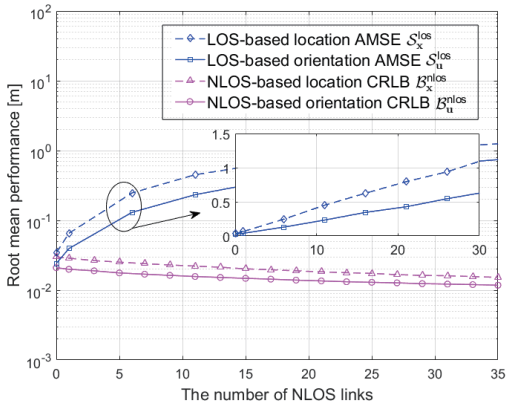

Fig. 8. VLP error v.s. the number of NLOS links.

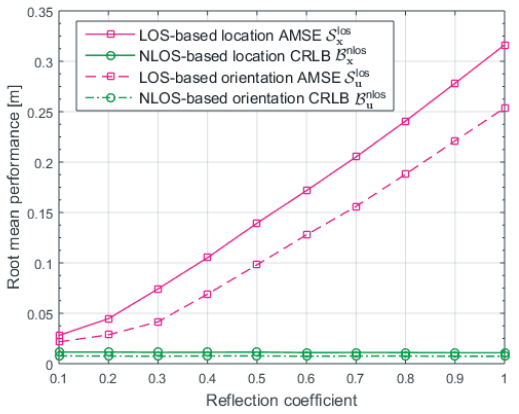

Fig. 9. VLP error v.s. the reflection coefficient

2) The Effect of NLOS Propagation: The LOS- and NLOS-based VLP error performances v.s. the number of NLOS links are given in Fig. 8. It is shown that the larger number of the NLOS links leads to the larger localization error for the LOS-based VLP method, which complies with Corollary 10. In contrast, for NLOS-based VLP method, the localization error will slightly reduce with the number of NLOS links since more NLOS links bring more UD location information to VLP, which complies with Corollary 9. This means that the NLOS-based VLP method can be expected to achieve a reliable solution in diffuse scattering environments via exploiting NLOS propagation knowledge.

3) The Impact of Reflection Coefficients: The localization performances of LOS- and NLOS-based VLP methods v.s. the reflection coefficients $\{\wp_{l,m}\}$ of NLOS channels are presented in Fig. 9, where we set $\wp_{l,m}$ ranges within [0.1,1] for all NLOS paths. It is shown that the LOS-based VLP error increases (almost linearly) with the reflection coefficient of the NLOS links. This is

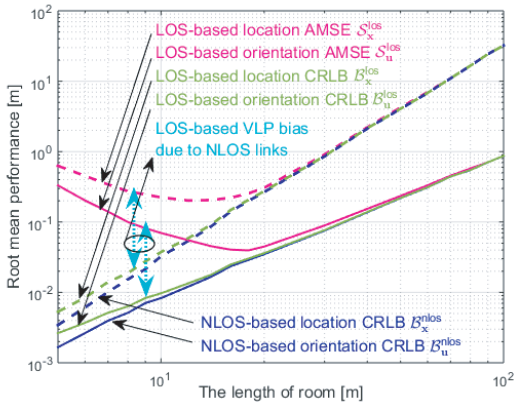

Fig. 10. VLP error performance v.s. the length of room.

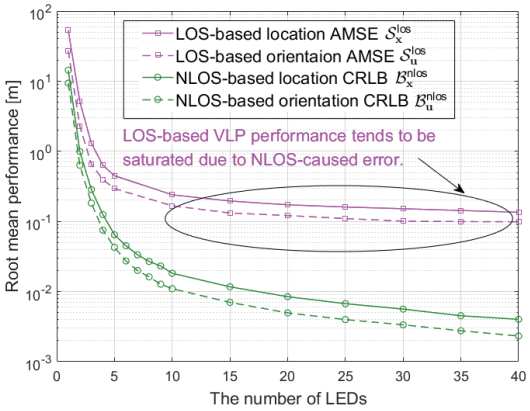

Fig. 11. The impact of the number of LEDs.

because a large refection coefficient leads to a large unaware NLOS component, as revealed in Theorem 2, 3 and Corollary 10. In contrast, the NLOS-based VLP error will not increase with an increasing reflection coefficient, due to the exploitation of NLOS propagation knowledge, which complies with Corollary 9.

4) The Effect of the Room Size: The VLP error performance v.s. the room size is assessed in Fig. 10, where we consider a cubic room with a length ranging from 5[m] to 100[m] and the LEDs are uniformly distributed on the room ceiling. The number of LEDs is fixed at 15. It is shown in Fig. 10 that the NLOS-based VLP error increases with the room size, which complies with Corollary 7. In contrast, the LOS-based VLP error first reduces and then increases with the room size. This is because a small NLOS path length will lead to a large NLOS interference, thus rendering a large VLP error, when the room size is small (e.g., less than 10 [m]).[10] As the room size increases, the NLOS path length increases, and hence the NLOS interference will rapidly reduce, and so does the gap between the LOS-based VLP error with its CRLB. Then, when the room size is sufficiently large, the LOS-based VLP error will tend to its CRLB, both are increasing with the room size. In this case, the scaling rate of the NLOS-based VLP error and LOS-based VLP error become the same.

5) The Impact of the Number of LEDs: The impact of $|\Theta_R|$ on the VLP performance is shown in Fig. 11, where $|\Theta_R|$ varies from 1 to 40 while the measurement noise strength is fixed at 10^{-8} (equivalent to an SNR around 30 dB for the case of 15 LEDs). We can see that the LOS-based VLP error will reduce and then tend to be saturated as $|\Theta_R|$ increases. This is due to the NLOS

[10]The strength of the NLOS component increases with the reduction of the NLOS path length, as shown in (4).

propagation-caused VLP error which cannot be reduced by deploying more LEDs. In contrast, the NLOS-based VLP error reduces with $|\Theta_R|$, which complies with Corollary 8. In addition, 10 LED arrays are enough for achieving a satisfactory VLP performance. When $|\Theta_R| > 10$, the NLOS-based VLP performance gain from the increased LEDs will gradually become marginal due to the limited deployment area (room ceiling) of LEDs.

VII. Conclusions

In this paper, the performance limits of VLP methods in diffuse scattering environments are studied, where two typical VLP methods, i.e., the LOS-based and the NLOS-based VLP methods are investigated.

Firstly, the closed-form error bounds of these two typical VLP methods are quantified to gain insights into the VLP performance limits under diffuse scattering effects. It is shown that the LOS-based VLP error is affected by both the noise and the NLOS component in RSS measurements, while the NLOS-based VLP error is determined by the measurement noise only. Hence, there will be error floor in the LOS-based VLP method as SNR increases, and the error floor depends on the NLOS signal strength, which has been quantified in the paper. In contrast, the NLOS-based VLP method has no such error floor as SNR increases, since the propagation knowledge of NLOS signals is exploited in its UD localization.

Secondly, the effect of the NLOS propagation on the VLP performance limits is analyzed. To be specific, the performance gain of the NLOS-based VLP method (from harnessing the NLOS links) over the LOS-based VLP method is quantified. It is established that exploiting the NLOS propagation knowledge in UD localization can significantly improve the VLP performance, particularly in a high-SNR condition.

Appendix A
Proof of Theorem 1

Let $\boldsymbol{\beta}_{\mathrm{UD}} = [\mathbf{x}; \mathbf{u}]$ be the joint variable. We shall first derive the CRLB for the LOS-based estimate $\hat{\boldsymbol{\beta}}_{\mathrm{UD}}^{\mathsf{los}}$, and then we will derive the CRLBs for $\mathbf{x}$ and $\mathbf{u}$, respectively. Let $\boldsymbol{\upsilon}$ be the bias of $\hat{\boldsymbol{\beta}}_{\mathrm{UD}}^{\mathsf{los}}$ due to the NLOS effect, i.e., $\boldsymbol{\upsilon} = \mathbb{E}\{\hat{\boldsymbol{\beta}}_{\mathrm{UD}}^{\mathsf{los}}\} - \boldsymbol{\beta}_{\mathrm{UD}}$. Thus, the mean squared error of $\hat{\boldsymbol{\beta}}_{\mathrm{UD}}^{\mathsf{los}}$ can be formulated as $\mathbb{E}\{\|\hat{\boldsymbol{\beta}}_{\mathrm{UD}}^{\mathsf{los}} - \boldsymbol{\beta}_{\mathrm{UD}}\|_2^2\} = \|\boldsymbol{\upsilon}\|_2^2 + \underbrace{\mathbb{E}\{\|\hat{\boldsymbol{\beta}}_{\mathrm{UD}}^{\mathsf{los}} - \mathbb{E}\{\hat{\boldsymbol{\beta}}_{\mathrm{UD}}^{\mathsf{los}}\}\|_2^2\}}_{\mathrm{cov}(\hat{\boldsymbol{\beta}}_{\mathrm{UD}}^{\mathsf{los}})}$, where it should be noted

that $\mathbb{E}\{\|\boldsymbol{v}\|_2^2\} = \|\boldsymbol{v}\|_2^2$ and $\mathrm{cov}(\hat{\boldsymbol{\beta}}_{\mathrm{UD}}^{\mathsf{los}})$ is the covariance of estimate error, which is bounded from above, i.e., $\mathrm{cov}(\hat{\boldsymbol{\beta}}_{\mathrm{UD}}^{\mathsf{los}}) \geq \mathrm{trace}\Big(\boldsymbol{\mathcal{B}}_{\boldsymbol{\beta}_{\mathrm{UD}}}^{\mathsf{los}}(\boldsymbol{\beta}_{\mathrm{UD}})\Big)$, where $\boldsymbol{\mathcal{B}}_{\boldsymbol{\beta}_{\mathrm{UD}}}^{\mathsf{los}}(\boldsymbol{\beta}_{\mathrm{UD}}) = \Big(\boldsymbol{\mathcal{I}}_{\boldsymbol{\beta}_{\mathrm{UD}}}^{\mathsf{los}}(\boldsymbol{\beta}_{\mathrm{UD}})\Big)^{-1}$, where $\boldsymbol{\mathcal{B}}_{\boldsymbol{\beta}_{\mathrm{UD}}}^{\mathsf{los}}(\boldsymbol{\beta}_{\mathrm{UD}}) \in \mathbb{S}^6$ is the CRLB of joint variable $\boldsymbol{\beta}_{\mathrm{UD}}$, and $\boldsymbol{\mathcal{I}}_{\boldsymbol{\beta}_{\mathrm{UD}}}^{\mathsf{los}}(\boldsymbol{\beta}_{\mathrm{UD}})$ is the FIM [32], given by $\boldsymbol{\mathcal{I}}_{\boldsymbol{\beta}_{\mathrm{UD}}}^{\mathsf{los}}(\boldsymbol{\beta}_{\mathrm{UD}}) = -\mathbb{E}_{\mathbf{z}|\boldsymbol{\beta}_{\mathrm{UD}}}\Big\{\nabla_{\boldsymbol{\beta}_{\mathrm{UD}}}^2 \ln p_{\mathsf{los}}(\mathbf{z}|\boldsymbol{\beta}_{\mathrm{UD}})\Big\}$, where $\nabla_{\boldsymbol{\beta}_{\mathrm{UD}}}^2(\bullet)$ is the second-order derivative w.r.t. $\boldsymbol{\beta}_{\mathrm{UD}}$, and $p_{\mathsf{los}}(\mathbf{z}|\boldsymbol{\beta}_{\mathrm{UD}}) = \mathcal{N}(\mathbf{z}|\mathbf{G}_{\mathsf{los}}(\mathbf{x})\boldsymbol{\mu}(\mathbf{u}) + \boldsymbol{\varsigma}_{\mathsf{nlos}}, \omega\mathbf{I}_{M_E|\Omega_R|})$, where $\boldsymbol{\mu}(\mathbf{u}) = \dfrac{\mathbf{u}}{\|\mathbf{u}\|_2}$.

Then, the FIM $\boldsymbol{\mathcal{I}}_{\boldsymbol{\beta}_{\mathrm{UD}}}^{\mathsf{los}}(\boldsymbol{\beta}_{\mathrm{UD}})$ will be eventually given by $\boldsymbol{\mathcal{I}}_{\boldsymbol{\beta}_{\mathrm{UD}}}^{\mathsf{los}}(\boldsymbol{\beta}_{\mathrm{UD}}) = \begin{bmatrix} \boldsymbol{\mathcal{I}}_{\mathbf{x},\mathbf{x}}^{\mathsf{los}}(\mathbf{x},\mathbf{u}) & \boldsymbol{\mathcal{I}}_{\mathbf{x},\mathbf{u}}^{\mathsf{los}}(\mathbf{x},\mathbf{u}) \\ \boldsymbol{\mathcal{I}}_{\mathbf{u},\mathbf{x}}^{\mathsf{los}}(\mathbf{x},\mathbf{u}) & \boldsymbol{\mathcal{I}}_{\mathbf{u},\mathbf{u}}^{\mathsf{los}}(\mathbf{x},\mathbf{u}) \end{bmatrix}$, where each 3×3 information element matrix is given by

$$\boldsymbol{\mathcal{I}}_{\mathbf{x},\mathbf{x}}^{\mathsf{los}}(\mathbf{x},\mathbf{u}) = \omega\mathbf{H}_{\mathsf{los}}(\mathbf{x})\mathbf{U}(\mathbf{u})\mathbf{U}^{\top}(\mathbf{u})\mathbf{H}_{\mathsf{los}}^{\top}(\mathbf{x}), \quad \boldsymbol{\mathcal{I}}_{\mathbf{x},\mathbf{u}}^{\mathsf{los}}(\mathbf{x},\mathbf{u}) = \omega\mathbf{H}_{\mathsf{los}}(\mathbf{x})\mathbf{U}(\mathbf{u})\mathbf{G}_{\mathsf{los}}(\mathbf{x})\boldsymbol{\mathcal{R}}^{\top}(\mathbf{u}), \quad (42)$$

$$\boldsymbol{\mathcal{I}}_{\mathbf{u},\mathbf{x}}^{\mathsf{los}}(\mathbf{x},\mathbf{u}) = \boldsymbol{\mathcal{I}}_{\mathbf{x},\mathbf{u}}^{\top}(\mathbf{x},\mathbf{u}), \quad \boldsymbol{\mathcal{I}}_{\mathbf{u},\mathbf{u}}^{\mathsf{los}}(\mathbf{x},\mathbf{u}) = \omega\boldsymbol{\mathcal{R}}(\mathbf{u})\mathbf{G}_{\mathsf{los}}^{\top}(\mathbf{x})\mathbf{G}_{\mathsf{los}}(\mathbf{x})\boldsymbol{\mathcal{R}}^{\top}(\mathbf{u}), \quad (43)$$

and $\mathbf{H}_{\mathsf{los}}(\mathbf{x})$, $\mathbf{U}(\mathbf{u})$, $\boldsymbol{\mathcal{R}}(\mathbf{u})$ and $\mathbf{G}_{\mathsf{los}}(\mathbf{x})$ are given by (12), (13), (15) and (6), respectively. Then, based on the structure of $\boldsymbol{\beta}_{\mathrm{UD}}$'s CRLB and using Schur complement [30], the CRLBs of $\mathbf{x}$ and $\mathbf{u}$ is eventually given by (10) and (11), respectively. Hence, Theorem 1 is proved.

APPENDIX B
PROOF OF THEOREM 2

In LOS-based VLP method, only LOS channel is exploited. Hence, its system model is recast as $\mathbf{z} = \mathbf{G}_{\mathsf{los}}(\mathbf{x})\boldsymbol{\mu}(\mathbf{u}) + \boldsymbol{\varsigma}_{\mathsf{nlos}} + \boldsymbol{\epsilon}$, where $\boldsymbol{\varsigma}_{\mathsf{nlos}} = \mathbf{G}_{\mathsf{nlos}}(\mathbf{x})\boldsymbol{\mu}(\mathbf{u})$ is the NLOS component but unaware for the LOS-based VLP. Let $\hat{\mathbf{z}} = \mathbf{G}_{\mathsf{los}}(\hat{\mathbf{x}}_{\mathsf{los}})\boldsymbol{\mu}(\hat{\mathbf{u}}_{\mathsf{los}})$ be the measurement guess of the LOS-based VLP method. Applying the first-order approximation around $\mathbf{x} = \mathbf{x}_{\mathsf{true}}$, where $\mathbf{x}_{\mathsf{true}}$ is the true value of $\mathbf{x}$, we obtain $\hat{\mathbf{z}} \approx \mathbf{G}_{\mathsf{los}}(\mathbf{x}_{\mathsf{true}})\boldsymbol{\mu}(\mathbf{u}_{\mathsf{true}}) + \begin{bmatrix} \nabla_{\mathbf{x}}\Big(\mathbf{G}_{\mathsf{los}}(\mathbf{x}_{\mathsf{true}})\boldsymbol{\mu}(\mathbf{u}_{\mathsf{true}})\Big) \\ \nabla_{\mathbf{u}}\Big(\mathbf{G}_{\mathsf{los}}(\mathbf{x}_{\mathsf{true}})\boldsymbol{\mu}(\mathbf{u}_{\mathsf{true}})\Big) \end{bmatrix}^{\top} \begin{bmatrix} \hat{\mathbf{x}}_{\mathsf{los}} - \mathbf{x}_{\mathsf{true}} \\ \hat{\mathbf{u}}_{\mathsf{los}} - \mathbf{u}_{\mathsf{true}} \end{bmatrix}$ where the high-order infinitesimal error of $\mathcal{O}\Big(\|\hat{\mathbf{x}}_{\mathsf{los}} - \mathbf{x}\|_2^2 + \|\hat{\mathbf{u}}_{\mathsf{los}} - \mathbf{u}\|_2^2\Big)$ is ignored. In addition, let $\boldsymbol{\varsigma}_{\mathsf{resi}} = \mathbf{z} - \hat{\mathbf{z}}$ be the residual measurement error of the LOS-based VLP, and let $\boldsymbol{\varsigma}_{\mathsf{bias}} = \boldsymbol{\varsigma}_{\mathsf{nlos}} - \boldsymbol{\varsigma}_{\mathsf{resi}}$. Since we know $\mathbf{z} = \mathbf{G}_{\mathsf{los}}(\mathbf{x}_{\mathsf{true}})\boldsymbol{\mu}(\mathbf{u}_{\mathsf{true}}) + \boldsymbol{\varsigma}_{\mathsf{nlos}} + \boldsymbol{\epsilon}$, we have

$$\begin{bmatrix} \nabla_{\mathbf{x}}\Big(\mathbf{G}_{\mathsf{los}}(\mathbf{x}_{\mathsf{true}})\boldsymbol{\mu}(\mathbf{u}_{\mathsf{true}})\Big) \\ \nabla_{\mathbf{u}}\Big(\mathbf{G}_{\mathsf{los}}(\mathbf{x}_{\mathsf{true}})\boldsymbol{\mu}(\mathbf{u}_{\mathsf{true}})\Big) \end{bmatrix}^{\top} \begin{bmatrix} \hat{\mathbf{x}}_{\mathsf{los}} - \mathbf{x}_{\mathsf{true}} \\ \hat{\mathbf{u}}_{\mathsf{los}} - \mathbf{u}_{\mathsf{true}} \end{bmatrix} \approx \boldsymbol{\varsigma}_{\mathsf{bias}} + \boldsymbol{\epsilon}. \quad (44)$$

Taking the expectation over $\boldsymbol{\epsilon}$, we have $\begin{bmatrix} \nabla_{\mathbf{x}}\Big(\mathbf{G}_{\mathsf{los}}(\mathbf{x}_{\mathsf{true}})\boldsymbol{\mu}(\mathbf{u}_{\mathsf{true}})\Big) \\ \nabla_{\mathbf{u}}\Big(\mathbf{G}_{\mathsf{los}}(\mathbf{x}_{\mathsf{true}})\boldsymbol{\mu}(\mathbf{u}_{\mathsf{true}})\Big) \end{bmatrix}^{\top} \begin{bmatrix} \mathbb{E}\{\hat{\mathbf{x}}_{\mathsf{los}}\} - \mathbf{x}_{\mathsf{true}} \\ \mathbb{E}\{\hat{\mathbf{u}}_{\mathsf{los}}\} - \mathbf{u}_{\mathsf{true}} \end{bmatrix} \approx \boldsymbol{\varsigma}_{\mathsf{bias}}$, where we have assumed $\mathbb{E}\{\boldsymbol{\epsilon}\} = \mathbf{0}$. As a result, we arrive at

$$\boldsymbol{\varsigma}_{\mathsf{bias}}\boldsymbol{\varsigma}_{\mathsf{bias}}^{\top} \approx \begin{bmatrix} \nabla_{\mathbf{x}}^{\top}\Big(\mathbf{G}_{\mathsf{los}}(\mathbf{x}_{\mathsf{true}})\boldsymbol{\mu}(\mathbf{u}_{\mathsf{true}})\Big) \\ \nabla_{\mathbf{u}}^{\top}\Big(\mathbf{G}_{\mathsf{los}}(\mathbf{x}_{\mathsf{true}})\boldsymbol{\mu}(\mathbf{u}_{\mathsf{true}})\Big) \end{bmatrix} \begin{bmatrix} \mathbb{E}\{\hat{\mathbf{x}}_{\mathsf{los}}\} - \mathbf{x}_{\mathsf{true}} \\ \mathbb{E}\{\hat{\mathbf{u}}_{\mathsf{los}}\} - \mathbf{u}_{\mathsf{true}} \end{bmatrix} \begin{bmatrix} \mathbb{E}\{\hat{\mathbf{x}}_{\mathsf{los}}\} - \mathbf{x}_{\mathsf{true}} \\ \mathbb{E}\{\hat{\mathbf{u}}_{\mathsf{los}}\} - \mathbf{u}_{\mathsf{true}} \end{bmatrix}^{\top} \begin{bmatrix} \nabla_{\mathbf{x}}\Big(\mathbf{G}_{\mathsf{los}}(\mathbf{x}_{\mathsf{true}})\boldsymbol{\mu}(\mathbf{u}_{\mathsf{true}})\Big) \\ \nabla_{\mathbf{u}}\Big(\mathbf{G}_{\mathsf{los}}(\mathbf{x}_{\mathsf{true}})\boldsymbol{\mu}(\mathbf{u}_{\mathsf{true}})\Big) \end{bmatrix}. \quad (45)$$

It should be noted that $\nabla_{\mathbf{x}}\Big(\mathbf{G}_{\mathsf{los}}(\mathbf{x}_{\mathsf{true}})\boldsymbol{\mu}(\mathbf{u}_{\mathsf{true}})\Big) = \mathbf{H}_{\mathsf{los}}(\mathbf{x})\mathbf{U}(\mathbf{u})$ and $\upsilon_{\mathbf{x}} = \|\mathbb{E}\{\hat{\mathbf{x}}_{\mathsf{los}}\} - \mathbf{x}_{\mathsf{true}}\|_2$. Hence, taking the trace of the 3×3 left-top submatrix and the 3×3 right-bottom submatrix of the correlation matrix $\boldsymbol{\varsigma}_{\mathsf{bias}}\boldsymbol{\varsigma}_{\mathsf{bias}}^{\top}$ in (45), respectively, and using the singular-value-decomposition of the left coefficient matrix, Theorem 2 is proved.

APPENDIX C
PROOF OF THEOREM 3

Let $\boldsymbol{\epsilon}_{\mathsf{overall}} = \boldsymbol{\varsigma}_{\mathsf{bias}} + \boldsymbol{\epsilon}$. Then, as per (44), we have

$$\mathbb{E}\{\boldsymbol{\epsilon}_{\mathsf{overall}}\boldsymbol{\epsilon}_{\mathsf{overall}}^{\top}\} \approx \mathbb{E}\left\{ \begin{bmatrix} \nabla_{\mathbf{x}}^{\top}\Big(\mathbf{G}_{\mathsf{los}}(\mathbf{x}_{\mathsf{true}})\boldsymbol{\mu}(\mathbf{u}_{\mathsf{true}})\Big) \\ \nabla_{\mathbf{u}}^{\top}\Big(\mathbf{G}_{\mathsf{los}}(\mathbf{x}_{\mathsf{true}})\boldsymbol{\mu}(\mathbf{u}_{\mathsf{true}})\Big) \end{bmatrix} \begin{bmatrix} \hat{\mathbf{x}}_{\mathsf{los}} - \mathbf{x}_{\mathsf{true}} \\ \hat{\mathbf{u}}_{\mathsf{los}} - \mathbf{u}_{\mathsf{true}} \end{bmatrix} \begin{bmatrix} \hat{\mathbf{x}}_{\mathsf{los}} - \mathbf{x}_{\mathsf{true}} \\ \hat{\mathbf{u}}_{\mathsf{los}} - \mathbf{u}_{\mathsf{true}} \end{bmatrix}^{\top} \begin{bmatrix} \nabla_{\mathbf{x}}\Big(\mathbf{G}_{\mathsf{los}}(\mathbf{x}_{\mathsf{true}})\boldsymbol{\mu}(\mathbf{u}_{\mathsf{true}})\Big) \\ \nabla_{\mathbf{u}}\Big(\mathbf{G}_{\mathsf{los}}(\mathbf{x}_{\mathsf{true}})\boldsymbol{\mu}(\mathbf{u}_{\mathsf{true}})\Big) \end{bmatrix} \right\},$$

and we further arrive at

$$\mathbb{E}\left\{ \begin{bmatrix} \hat{\mathbf{x}}_{\mathsf{los}} - \mathbf{x}_{\mathsf{true}} \\ \hat{\mathbf{u}}_{\mathsf{los}} - \mathbf{u}_{\mathsf{true}} \end{bmatrix} \begin{bmatrix} \hat{\mathbf{x}}_{\mathsf{los}} - \mathbf{x}_{\mathsf{true}} \\ \hat{\mathbf{u}}_{\mathsf{los}} - \mathbf{u}_{\mathsf{true}} \end{bmatrix}^{\top} \right\} \approx \begin{bmatrix} \mathbf{U}^{\top}(\mathbf{u}_{\mathsf{true}})\mathbf{H}_{\mathsf{los}}^{\top}(\mathbf{x}_{\mathsf{true}}) \\ \boldsymbol{\mathcal{R}}(\mathbf{u}_{\mathsf{true}})\mathbf{G}_{\mathsf{los}}^{\top}(\mathbf{x}_{\mathsf{true}}) \end{bmatrix}^{\dagger} \mathbb{E}\{\boldsymbol{\varsigma}_{\mathsf{bias}}\boldsymbol{\varsigma}_{\mathsf{bias}}^{\top}\} \begin{bmatrix} \mathbf{H}_{\mathsf{los}}(\mathbf{x}_{\mathsf{true}})\mathbf{U}(\mathbf{u}_{\mathsf{true}}) \\ \mathbf{G}_{\mathsf{los}}(\mathbf{x}_{\mathsf{true}})\boldsymbol{\mathcal{R}}^{\top}(\mathbf{u}_{\mathsf{true}}) \end{bmatrix}^{\dagger}$$
$$+ \underbrace{\begin{bmatrix} \mathbf{U}^{\top}(\mathbf{u}_{\mathsf{true}})\mathbf{H}_{\mathsf{los}}^{\top}(\mathbf{x}_{\mathsf{true}}) \\ \mathbf{G}_{\mathsf{los}}(\mathbf{x}_{\mathsf{true}})\boldsymbol{\mathcal{R}}^{\top}(\mathbf{u}_{\mathsf{true}}) \end{bmatrix}^{\dagger} \mathbb{E}\{\boldsymbol{\epsilon}\boldsymbol{\epsilon}^{\top}\} \begin{bmatrix} \mathbf{H}_{\mathsf{los}}(\mathbf{x}_{\mathsf{true}})\mathbf{U}(\mathbf{u}_{\mathsf{true}}) \\ \boldsymbol{\mathcal{R}}(\mathbf{u}_{\mathsf{true}})\mathbf{G}_{\mathsf{los}}^{\top}(\mathbf{x}_{\mathsf{true}}) \end{bmatrix}^{\dagger}}_{\text{LOS-based CRLB}}. \quad (46)$$

Hence, taking the trace of the 3×3 left-top submatrix and the 3×3 right-bottom submatrix of the left-hand-side correlation matrix in (46), respectively, the equations in Theorem 3 are obtained. An approximation with an error of $\mathcal{O}\Big(\|\hat{\mathbf{x}}_{\mathsf{los}}-\mathbf{x}_{\mathsf{true}}\|_2^2 + \|\hat{\mathbf{u}}_{\mathsf{los}}-\mathbf{u}_{\mathsf{true}}\|_2^2\Big)$ is employed in (44), and hence the LOS-based VLP performance approximation error is $\mathcal{O}\Big(\|\hat{\mathbf{x}}_{\mathsf{los}}-\mathbf{x}_{\mathsf{true}}\|_2^2+\|\hat{\mathbf{u}}_{\mathsf{los}}-\mathbf{u}_{\mathsf{true}}\|_2^2\Big)$.

APPENDIX D
PROOF OF THEOREM 4

The derivation of the NLOS-based CRLBs follows from a similar idea to the LOS-based CRLBs given in (10) and (11), where we only need to replay $\mathbf{G}_{\mathsf{los}}(\mathbf{x})$ by $\mathbf{G}(\mathbf{x})$ and hence all FIMs should relate to the NLOS-based information elements. As per the FIM definition in Appendix A, the NLOS-based FIM $\boldsymbol{\mathcal{I}}_{\boldsymbol{\alpha}}(\boldsymbol{\beta}_{\mathrm{UD}})$ is structured as $\boldsymbol{\mathcal{I}}_{\boldsymbol{\alpha}}(\boldsymbol{\beta}_{\mathrm{UD}}) = \begin{bmatrix} \boldsymbol{\mathcal{I}}_{\mathbf{x},\mathbf{x}} & \boldsymbol{\mathcal{I}}_{\mathbf{x},\mathbf{u}} & \boldsymbol{\mathcal{I}}_{\mathbf{x},\mathbf{s}} & \boldsymbol{\mathcal{I}}_{\mathbf{x},\boldsymbol{\wp}} \\ \boldsymbol{\mathcal{I}}_{\mathbf{u},\mathbf{x}} & \boldsymbol{\mathcal{I}}_{\mathbf{u},\mathbf{u}} & \boldsymbol{\mathcal{I}}_{\mathbf{u},\mathbf{s}} & \boldsymbol{\mathcal{I}}_{\mathbf{u},\boldsymbol{\wp}} \\ \boldsymbol{\mathcal{I}}_{\mathbf{s},\mathbf{x}} & \boldsymbol{\mathcal{I}}_{\mathbf{s},\mathbf{u}} & \boldsymbol{\mathcal{I}}^{\mathsf{nlos}}_{\mathbf{s},\mathbf{s}} & \boldsymbol{\mathcal{I}}^{\mathsf{nlos}}_{\mathbf{s},\boldsymbol{\wp}} \\ \boldsymbol{\mathcal{I}}_{\boldsymbol{\wp},\mathbf{x}} & \boldsymbol{\mathcal{I}}_{\boldsymbol{\wp},\mathbf{u}} & \boldsymbol{\mathcal{I}}^{\mathsf{nlos}}_{\boldsymbol{\wp},\mathbf{s}} & \boldsymbol{\mathcal{I}}^{\mathsf{nlos}}_{\boldsymbol{\wp},\boldsymbol{\wp}} \end{bmatrix}$, where each information element is given by

$$\boldsymbol{\mathcal{I}}_{\mathbf{x},\mathbf{x}} \in \mathbb{S}^3 = \omega \mathbf{H}(\mathbf{x})\mathbf{U}(\mathbf{u})\mathbf{U}^\top(\mathbf{u})\mathbf{H}^\top(\mathbf{x}), \quad \boldsymbol{\mathcal{I}}_{\mathbf{x},\mathbf{u}} \in \mathbb{R}^{3\times 3} = \omega \mathbf{H}(\mathbf{x})\mathbf{U}(\mathbf{u})\mathbf{G}(\mathbf{x})\boldsymbol{\mathcal{R}}^\top(\mathbf{u}), \tag{47}$$

$$\boldsymbol{\mathcal{I}}_{\mathbf{x},\mathbf{s}} \in \mathbb{R}^{3\times 3L|\Omega_R|} = \omega \mathbf{H}(\mathbf{x})\mathbf{U}(\mathbf{u})\mathbf{U}^\top(\mathbf{u})\boldsymbol{\mathcal{H}}^\top_{\mathsf{nlos}}(\mathbf{x}), \quad \boldsymbol{\mathcal{I}}_{\mathbf{x},\boldsymbol{\wp}} \in \mathbb{R}^{3\times L|\Omega_R|} = \omega \mathbf{H}(\mathbf{x})\mathbf{U}(\mathbf{u})\mathbf{K}_{\mathsf{nlos}}(\mathbf{x},\mathbf{u}),$$

$$\boldsymbol{\mathcal{I}}_{\mathbf{u},\mathbf{u}} \in \mathbb{S}^3 = \omega \boldsymbol{\mathcal{R}}(\mathbf{u})\mathbf{G}^\top(\mathbf{x})\mathbf{G}(\mathbf{x})\boldsymbol{\mathcal{R}}^\top(\mathbf{u}) \quad \boldsymbol{\mathcal{I}}_{\mathbf{u},\mathbf{s}} \in \mathbb{R}^{3\times 3L|\Omega_R|} = \omega \boldsymbol{\mathcal{R}}(\mathbf{u})\mathbf{G}^\top(\mathbf{x})\mathbf{U}^\top(\mathbf{u})\boldsymbol{\mathcal{H}}^\top_{\mathsf{nlos}}(\mathbf{x}),$$

$$\boldsymbol{\mathcal{I}}_{\mathbf{u},\boldsymbol{\wp}} \in \mathbb{R}^{3\times L|\Omega_R|} = \omega \boldsymbol{\mathcal{R}}(\mathbf{u})\mathbf{G}^\top(\mathbf{x})\mathbf{K}_{\mathsf{nlos}}(\mathbf{x},\mathbf{u}), \quad \boldsymbol{\mathcal{I}}^{\mathsf{nlos}}_{\mathbf{s},\mathbf{s}} \in \mathbb{S}^{3L|\Omega_R|} = \omega \boldsymbol{\mathcal{H}}_{\mathsf{nlos}}(\mathbf{x})\mathbf{U}(\mathbf{u})\mathbf{U}^\top(\mathbf{u})\boldsymbol{\mathcal{H}}^\top_{\mathsf{nlos}}(\mathbf{x}),$$

$$\boldsymbol{\mathcal{I}}^{\mathsf{nlos}}_{\mathbf{s},\boldsymbol{\wp}} \in \mathbb{R}^{3L|\Omega_R|\times L|\Omega_R|} = \omega \boldsymbol{\mathcal{H}}_{\mathsf{nlos}}(\mathbf{x})\mathbf{U}(\mathbf{u})\mathbf{K}_{\mathsf{nlos}}(\mathbf{x},\mathbf{u}), \quad \boldsymbol{\mathcal{I}}^{\mathsf{nlos}}_{\boldsymbol{\wp},\boldsymbol{\wp}} \in \mathbb{S}^{L|\Omega_R|} = \omega \mathbf{K}^\top_{\mathsf{nlos}}(\mathbf{x},\mathbf{u})\mathbf{K}_{\mathsf{nlos}}(\mathbf{x},\mathbf{u}),$$

where $\boldsymbol{\mathcal{H}}_{\mathsf{nlos}}(\mathbf{x}) \in \mathbb{R}^{3L|\Omega_R|\times 3M_E|\Omega_R|}$ is given by $\boldsymbol{\mathcal{H}}_{\mathsf{nlos}}(\mathbf{x}) = [\boldsymbol{\mathcal{H}}_{k,m}|\forall k = 1:M_E, \forall m \in \Omega_R]$ with $\boldsymbol{\mathcal{H}}_{k,m} = \mathsf{mat}\,[\,\boldsymbol{\mathcal{H}}_{k,m;m'}|\forall m' \in \Omega_R]$ and $\boldsymbol{\mathcal{H}}_{k,m;m'} \in \mathbb{C}^{3L\times 3} = \begin{cases} \boldsymbol{\mathcal{H}}'_{k,m}, & \text{if } m' = m, \\ \mathbf{0}_{3L\times 3}, & \text{otherwidse}, \end{cases}$, where $\boldsymbol{\mathcal{H}}'_{k,m} = \mathsf{mat}\,[\,\boldsymbol{\mathcal{H}}'_{l,k,m}|\forall l = 1:L]$, and $\boldsymbol{\mathcal{H}}'_{l,k,m} \in \mathbb{R}^{3\times 3}$ is given by

$$\begin{aligned} \boldsymbol{\mathcal{H}}'_{l,k,m} = {} & \Psi_R \frac{r(r+1)^2}{2\pi} \frac{\wp_{l,m}\left((\mathbf{s}_{l,m}-\mathbf{p}_{k,m})^\top \mathbf{v}_{k,m}\right)^{r-1}}{\|\mathbf{s}_{l,m}-\mathbf{p}_{k,m}\|_2^{r+2}\|\mathbf{s}_{l,m}-\mathbf{x}\|_2^3}\mathbf{v}_{k,m}(\mathbf{s}_{l,m}-\mathbf{x})^\top \\ & - \Psi_R \frac{(r+2)(r+1)^2}{2\pi} \frac{\wp_{l,m}\varphi_{l,k,m}}{\|\mathbf{s}_{l,m}-\mathbf{p}_{k,m}\|_2^2\|\mathbf{s}_{l,m}-\mathbf{x}\|_2^3}(\mathbf{s}_{l,m}-\mathbf{p}_m)(\mathbf{s}_{l,m}-\mathbf{x})^\top \\ & + \Psi_R \frac{(r+1)^2}{2\pi} \frac{\wp_{l,m}\varphi_{l,k,m}}{\|\mathbf{x}-\mathbf{s}_{l,m}\|_2^3}\mathbf{I}_3 - \Psi_R \frac{3(r+1)^2}{4\pi^2} \frac{\wp_{l,m}\varphi_{l,k,m}}{\|\mathbf{x}-\mathbf{s}_{l,m}\|_2^5}(\mathbf{s}_{l,m}-\mathbf{x})(\mathbf{s}_{l,m}-\mathbf{x})^\top. \end{aligned} \tag{48}$$

In addition, $\mathbf{K}_{\mathsf{nlos}}(\mathbf{x},\mathbf{u}) \in \mathbb{R}^{M_E|\Omega_R|\times L|\Omega_R|}$ is $\mathbf{K}_{\mathsf{nlos}}(\mathbf{x},\mathbf{u}) = \mathsf{diag}[\mathbf{K}_m(\mathbf{x},\mathbf{u})|\forall m \in \Omega_R]$, where $\mathbf{K}_m(\mathbf{x},\mathbf{u}) = \mathsf{mat}[\mathbf{q}^\top_{k,m}(\mathbf{x},\mathbf{u})|\forall k = 1:M_E]$, and $\mathbf{q}_{k,m}(\mathbf{x},\mathbf{u}) = \mathsf{vec}[q_{l,k,m}|\forall l = 1:L]$, in which

$q_{l,k,m} \in \mathbb{R} = \Psi_R \dfrac{(r+1)^2 \left((\mathbf{s}_{l,m}-\mathbf{p}_{k,m})^\top \mathbf{v}_{k,m}\right)^r (\mathbf{s}_{l,m}-\mathbf{x})^\top \mathbf{u}}{2\pi \|\mathbf{s}_{l,m}-\mathbf{p}_{k,m}\|_2^{r+2} \|\mathbf{x}-\mathbf{s}_{l,m}\|_2^3}$. Based on the structure of $\boldsymbol{\mathcal{I}}_{\boldsymbol{\alpha}}(\boldsymbol{\beta}_{\rm UD})$, applying the Schur complement, the UD location-based FIM is given by

$$\boldsymbol{\mathcal{Q}}_{\mathbf{x}}^{\mathsf{nlos}}(\boldsymbol{\beta}_{\rm UD}) = \boldsymbol{\mathcal{I}}_{\mathbf{x},\mathbf{x}} - \boldsymbol{\mathcal{P}}_{\mathbf{x}} \mathbf{W}_{\mathbf{x}}^{-1} \boldsymbol{\mathcal{P}}_{\mathbf{x}}^\top, = \omega \mathbf{H}(\mathbf{x}) \mathbf{U}(\mathbf{u}) \mathbf{U}^\top(\mathbf{u}) \mathbf{H}^\top(\mathbf{x}) - \boldsymbol{\mathcal{P}}_{\mathbf{x}} \mathbf{W}_{\mathbf{x}}^{-1} \boldsymbol{\mathcal{P}}_{\mathbf{x}}^\top, \tag{49}$$

where $\boldsymbol{\mathcal{P}}_{\mathbf{x}} \in \mathbb{R}^{3\times(4L|\Omega_R|+3)}$ and $\mathbf{W}_{\mathbf{x}} \in \mathbb{S}^{(4L|\Omega_R|+3)}$ are given by

$$\boldsymbol{\mathcal{P}}_{\mathbf{x}} = \begin{bmatrix} \boldsymbol{\mathcal{I}}_{\mathbf{x},\mathbf{u}} & \boldsymbol{\mathcal{I}}_{\mathbf{x},\mathbf{s}} & \boldsymbol{\mathcal{I}}_{\mathbf{x},\wp} \end{bmatrix}, \qquad \mathbf{W}_{\mathbf{x}} = \begin{bmatrix} \boldsymbol{\mathcal{I}}_{\mathbf{u},\mathbf{u}} & \boldsymbol{\mathcal{I}}_{\mathbf{u},\mathbf{s}} & \boldsymbol{\mathcal{I}}_{\mathbf{u},\wp} \\ \boldsymbol{\mathcal{I}}_{\mathbf{s},\mathbf{u}} & \boldsymbol{\mathcal{I}}_{\mathbf{s},\mathbf{s}}^{\mathsf{nlos}} & \boldsymbol{\mathcal{I}}_{\mathbf{s},\wp}^{\mathsf{nlos}} \\ \boldsymbol{\mathcal{I}}_{\wp,\mathbf{u}} & \boldsymbol{\mathcal{I}}_{\wp,\mathbf{s}}^{\mathsf{nlos}} & \boldsymbol{\mathcal{I}}_{\wp,\wp}^{\mathsf{nlos}} \end{bmatrix}, \tag{50}$$

and each information element $\boldsymbol{\mathcal{I}}_{\bullet,\bullet}$ has been given by (47).

Rearranging $\boldsymbol{\mathcal{I}}_{\boldsymbol{\alpha}}(\boldsymbol{\beta}_{\rm UD})$ and applying the Schur complement, the UD orientation-based FIM $\boldsymbol{\mathcal{Q}}_{\mathbf{u}}^{\mathsf{nlos}}(\boldsymbol{\beta}_{\rm UD})$ is given by $\boldsymbol{\mathcal{Q}}_{\mathbf{u}}^{\mathsf{nlos}}(\boldsymbol{\beta}_{\rm UD}) = \boldsymbol{\mathcal{I}}_{\mathbf{u},\mathbf{u}} - \boldsymbol{\mathcal{P}}_{\mathbf{u}} \mathbf{W}_{\mathbf{u}}^{-1} \boldsymbol{\mathcal{P}}_{\mathbf{u}}^\top = \boldsymbol{\mathcal{R}}(\mathbf{u}) \mathbf{G}^\top(\mathbf{x}) \mathbf{G}(\mathbf{x}) \boldsymbol{\mathcal{R}}^\top(\mathbf{u}) - \boldsymbol{\mathcal{P}}_{\mathbf{u}} \mathbf{W}_{\mathbf{u}}^{-1} \boldsymbol{\mathcal{P}}_{\mathbf{u}}^\top$, where $\boldsymbol{\mathcal{P}}_{\mathbf{u}} \in \mathbb{R}^{3\times(4L|\Omega_R|+3)}$ and $\mathbf{W}_{\mathbf{u}} \in \mathbb{S}^{(4L|\Omega_R|+3)}$ are given by

$$\boldsymbol{\mathcal{P}}_{\mathbf{u}} = \begin{bmatrix} \boldsymbol{\mathcal{I}}_{\mathbf{u},\mathbf{x}} & \boldsymbol{\mathcal{I}}_{\mathbf{u},\mathbf{s}} & \boldsymbol{\mathcal{I}}_{\mathbf{u},\wp} \end{bmatrix}, \qquad \mathbf{W}_{\mathbf{u}} = \begin{bmatrix} \boldsymbol{\mathcal{I}}_{\mathbf{x},\mathbf{x}} & \boldsymbol{\mathcal{I}}_{\mathbf{x},\mathbf{s}} & \boldsymbol{\mathcal{I}}_{\mathbf{x},\wp} \\ \boldsymbol{\mathcal{I}}_{\mathbf{s},\mathbf{x}} & \boldsymbol{\mathcal{I}}_{\mathbf{s},\mathbf{s}}^{\mathsf{nlos}} & \boldsymbol{\mathcal{I}}_{\mathbf{s},\wp}^{\mathsf{nlos}} \\ \boldsymbol{\mathcal{I}}_{\wp,\mathbf{x}} & \boldsymbol{\mathcal{I}}_{\wp,\mathbf{s}}^{\mathsf{nlos}} & \boldsymbol{\mathcal{I}}_{\wp,\wp}^{\mathsf{nlos}} \end{bmatrix}. \tag{51}$$

Hence, we arrive at $\mathfrak{B}_{\mathbf{x}}^{\mathsf{nlos}} = \left(\boldsymbol{\mathcal{Q}}_{\mathbf{x}}^{\mathsf{nlos}}(\boldsymbol{\beta}_{\rm UD})\right)^{-1}$ and $\mathfrak{B}_{\mathbf{u}}^{\mathsf{nlos}} = \left(\boldsymbol{\mathcal{Q}}_{\mathbf{u}}^{\mathsf{nlos}}(\boldsymbol{\beta}_{\rm UD})\right)^{-1}$. As per the estimation theory, the UD location and orientation errors will be bounded by the above CRLBs, respectively, as shown in (22) and (23). Hence, Theorem 4 is proved.

APPENDIX E
PROOF OF LEMMA 1

As per (46) in APPENDIX C, the LOS-based localization error covariance matrix follows that $\mathbb{E}\{(\hat{\mathbf{x}}_{\mathsf{los}}-\mathbf{x})(\hat{\mathbf{x}}_{\mathsf{los}}-\mathbf{x})^\top\} \approx \mathfrak{B}_{\mathbf{x}}^{\mathsf{los}} + \mathfrak{B}_{\mathbf{x}}^{\mathsf{bias}}$, where $\mathfrak{B}_{\mathbf{x}}^{\mathsf{bias}} = \|\boldsymbol{\varsigma}_{\mathsf{bias}}\|_2^2 \Big(\mathbf{H}_{\mathsf{los}}(\mathbf{x}) \mathbf{U}(\mathbf{u}) \mathbf{U}^\top(\mathbf{u})\, \mathbf{H}_{\mathsf{los}}^\top(\mathbf{x})\Big)^{-1}$. Then, given $\boldsymbol{\mathcal{J}}_{\mathbf{x}}^{\mathsf{bias}}$ defined in (33) and taking the inverse of both sides of the above correlation approximation, the LOS-based VLP information $\tilde{\boldsymbol{\mathcal{Q}}}_{\mathbf{x}}^{\mathsf{los}}$ can be approximated by $\boldsymbol{\mathcal{Q}}_{\mathbf{x}}^{\mathsf{los}}$ in (34).

APPENDIX F
PROOF OF COROLLARY 4

We know $\mathbf{H}(\mathbf{x}) = \mathbf{H}_{\mathsf{los}}(\mathbf{x}) + \mathbf{H}_{\mathsf{nlos}}(\mathbf{x})$, where $\mathbf{H}_{\mathsf{nlos}}(\mathbf{x})$ is gvien by (38), and hence $\boldsymbol{\mathcal{I}}_{\mathbf{x},\mathbf{x}}$ in (47) can also be cast as $\boldsymbol{\mathcal{I}}_{\mathbf{x},\mathbf{x}} = \omega\Big(\mathbf{H}_{\mathsf{los}}(\mathbf{x}) + \mathbf{H}_{\mathsf{nlos}}(\mathbf{x})\Big)\mathbf{U}(\mathbf{u})\mathbf{U}^{\top}(\mathbf{u})\Big(\mathbf{H}^{\top}_{\mathsf{los}}(\mathbf{x}) + \mathbf{H}^{\top}_{\mathsf{nlos}}(\mathbf{x})\Big)$. Therefore,

$$\begin{aligned}\boldsymbol{\mathcal{J}}_{\mathbf{x}}(\boldsymbol{\beta}_{\mathrm{UD}}) = & \underbrace{\omega\mathbf{H}_{\mathsf{los}}(\mathbf{x})\mathbf{U}(\mathbf{u})\mathbf{U}^{\top}(\mathbf{u})\mathbf{H}^{\top}_{\mathsf{los}}(\mathbf{x}) - \omega\mathbf{H}_{\mathsf{los}}(\mathbf{x})\mathbf{U}(\mathbf{u})\mathbf{F}^{\perp}_{\mathsf{los}}(\mathbf{x})\mathbf{U}^{\top}(\mathbf{u})\mathbf{H}^{\top}_{\mathsf{los}}(\mathbf{x})}_{\boldsymbol{\mathcal{J}}^{\mathsf{los}}_{\mathbf{x}}(\mathbf{x},\mathbf{u})} \\ & + \underbrace{\omega\mathbf{H}_{\mathsf{los}}(\mathbf{x})\mathbf{U}(\mathbf{u})\mathbf{U}^{\top}(\mathbf{u})\mathbf{H}^{\top}_{\mathsf{nlos}}(\mathbf{x}) + \omega\mathbf{H}_{\mathsf{nlos}}(\mathbf{x})\mathbf{U}(\mathbf{u})\mathbf{U}^{\top}(\mathbf{u})\Big(\mathbf{H}^{\top}_{\mathsf{los}}(\mathbf{x}) + \mathbf{H}^{\top}_{\mathsf{nlos}}(\mathbf{x})\Big)}_{\boldsymbol{\mathcal{D}}^{\mathsf{nlos}}_{\mathbf{x}}(\mathbf{x},\mathbf{u})} \\ & - \underbrace{\Big(\boldsymbol{\mathcal{P}}_{\mathbf{x}}\mathbf{W}_{\mathbf{x}}\boldsymbol{\mathcal{P}}^{\top}_{\mathbf{x}} - \omega\mathbf{H}_{\mathsf{los}}(\mathbf{x})\mathbf{U}(\mathbf{u})\mathbf{F}^{\perp}_{\mathsf{los}}(\mathbf{x})\mathbf{U}^{\top}(\mathbf{u})\mathbf{H}^{\top}_{\mathsf{los}}(\mathbf{x})\Big)}_{\boldsymbol{\mathcal{S}}^{\mathsf{nlos}}_{\mathbf{x}}(\mathbf{x},\mathbf{u})}. \end{aligned} \tag{52}$$

Hence, combining (52) with (36), the NLOS-based information $\boldsymbol{\mathcal{J}}^{\mathsf{nlos}}_{\mathbf{x}}(\mathbf{x},\mathbf{u})$ in (37) is obtained.

APPENDIX G
PROOF OF COROLLARY 7

Based on (47), (27) and (16), we know that $\boldsymbol{\mathcal{I}}_{\mathbf{x},\mathbf{x}}$ is $\mathcal{O}(\rho^{-6}_{\min})$, as $\rho_{\min} \to \infty$. We can observe from (47)–(48) and (50) that $\boldsymbol{\mathcal{P}}_{\mathbf{x}}\mathbf{W}^{-1}_{\mathbf{x}}\boldsymbol{\mathcal{P}}^{\top}_{\mathbf{x}}$ is $\mathcal{O}(\rho^{-6}_{\min})$. Hence, based on (49), we know $\boldsymbol{\mathcal{Q}}^{\mathsf{nlos}}_{\mathbf{x}}$ is $\mathcal{O}(\rho^{-6}_{\min})$. Thus, (40) is obtained. In the same way, based on (5), (6), (7), (3) and (4), we have $\boldsymbol{\mathcal{I}}_{\mathbf{u},\mathbf{u}} \sim \mathcal{O}(\rho^{-4}_{\min})$. Based on (51) and (47)–(48), we know $\boldsymbol{\mathcal{P}}_{\mathbf{u}}\mathbf{W}^{-1}_{\mathbf{u}}\boldsymbol{\mathcal{P}}^{\top}_{\mathbf{u}}$ is $\mathcal{O}(\rho^{-4}_{\min})$. Hence, we know $\boldsymbol{\mathcal{Q}}^{\mathsf{nlos}}_{\mathbf{u}}$ follows $\mathcal{O}(\rho^{-4}_{\min})$. Thus, (41) is obtained.

APPENDIX H
PROOF OF COROLLARY 8

Let us first consider the error bound $\boldsymbol{\mathfrak{B}}_{\boldsymbol{\alpha}}(\boldsymbol{\beta}_{\mathrm{UD}})$ of the joint variable $\boldsymbol{\alpha} = [\mathbf{x}, \mathbf{u}, \mathbf{s}, \wp]$, whose FIM $\boldsymbol{\mathcal{I}}_{\boldsymbol{\alpha}}(\boldsymbol{\beta}_{\mathrm{UD}})$ is given in (47)–(48). It can be easily verified that all information elements in $\boldsymbol{\mathcal{I}}_{\boldsymbol{\alpha}}(\boldsymbol{\beta}_{\mathrm{UD}})$ are $\Theta(|\Omega_R|)$. For instance, as shown in (47) and (27), the FIM element $\boldsymbol{\mathcal{I}}_{\mathbf{x},\mathbf{x}}$ follows $\mathbf{H}(\mathbf{x})\mathbf{U}(\mathbf{u})\mathbf{U}^{\top}(\mathbf{u})\mathbf{H}^{\top}(\mathbf{x}) = \sum\limits_{m\in\Omega_R}\mathbf{H}_m(\mathbf{x})\boldsymbol{\mu}(\mathbf{u})\boldsymbol{\mu}^{\top}(\mathbf{u})\mathbf{H}^{\top}_m(\mathbf{x})$, where $\mathbf{H}_m(\mathbf{x})$ is the mth component of $\mathbf{H}(\mathbf{x})$. Hence, if the LEDs are uniformly distributed, we have $\boldsymbol{\mathcal{I}}_{\boldsymbol{\alpha}}(\boldsymbol{\beta}_{\mathrm{UD}}) \sim \Theta(|\Omega_R|)$, and thus $\boldsymbol{\mathfrak{B}}_{\boldsymbol{\alpha}}(\boldsymbol{\beta}_{\mathrm{UD}}) \sim \Theta(|\Omega_R|^{-1})$ as $\boldsymbol{\mathfrak{B}}_{\boldsymbol{\alpha}}(\boldsymbol{\beta}_{\mathrm{UD}}) = (\boldsymbol{\mathcal{I}}_{\boldsymbol{\alpha}}(\boldsymbol{\beta}_{\mathrm{UD}}))^{-1}$. Since $\boldsymbol{\mathfrak{B}}^{\mathsf{nlos}}_{\mathbf{x}}(\mathbf{x},\mathbf{u})$ and $\boldsymbol{\mathfrak{B}}^{\mathsf{nlos}}_{\mathbf{u}}(\mathbf{x},\mathbf{u})$ is the top-left and right-bottom 3×3 submatrices, respectively, of $\boldsymbol{\mathfrak{B}}_{\boldsymbol{\alpha}}(\boldsymbol{\beta}_{\mathrm{UD}})$, both are $\Theta(|\Omega_R|^{-1})$.

APPENDIX I
PROOF OF COROLLARIES 9 AND 10

Firstly, we give the proof of Corollary 9. For the NLOS-based VLP method, as $\|\wp\|_2 \to \infty$, we have $\mathcal{D}_{\mathbf{x}}^{\mathsf{nlos}}(\mathbf{x},\mathbf{u}) \sim \mathcal{O}(\|\wp\|_2^2)$. Similarly, $\mathcal{S}_{\mathbf{x}}^{\mathsf{nlos}} \sim \mathcal{O}(\|\wp\|_2^2)$. Hence, based on (37), we know $\mathcal{J}_{\mathbf{x}}^{\mathsf{nlos}}(\mathbf{x},\mathbf{u}) \sim \mathcal{O}(\|\wp\|_2^2)$. Thus, Corollary 9 is proved.

Secondly, we give the proof of Corollary 10. For the LOS-based VLP method, as $\|\wp\|_2 \to \infty$, $\|\varsigma_{\mathsf{nlos}}\|_2^2 \sim \mathcal{O}(\|\wp\|_2^2)$, and hence based on (33) we have $\mathcal{J}_{\mathbf{x}}^{\mathsf{bias}}(\mathbf{x},\mathbf{u}) \sim \mathcal{O}(\|\wp\|_2^{-2})$.

REFERENCES

[1] E. Cardarelli, V. Digani, L. Sabattini, C. Secchi, and C. Fantuzzi, "Cooperative cloud robotics architecture for the coordination of multi-AGV systems in industrial warehouses." *Mechatronics*, 45 (2017): 1-13.

[2] R. Krug, T. Stoyanov, V. Tincani, H. Andreasson, R. Mosberger, G. Fantoni, and A. J. Lilienthal, "The next step in robot commissioning: Autonomous picking and palletizing." *IEEE Robotics and Automation Letters* 1.1 (2016): 546-553.

[3] J. Moon, I. Bae, and S. Kim. "Real-time near-optimal path and maneuver planning in automatic parking using a simultaneous dynamic optimization approach." *Intelligent Vehicles Symposium (IV)*, 2017 IEEE. IEEE, 2017.

[4] J. Armstrong, Y. A. Sekercioglu and A. Neild, "Vislbile Light Positioning: A Roadmap for international Standardization", *IEEE Communication Magzine*, Vol.51, No.12, 2013, pp.68-73.

[5] L. Yin, X. Wu and H. Haas, "Indoor Visible Light Positioning with Angle Diversity Transmitter." *2015 IEEE 82nd Vehicular Technology Conference (VTC Fall)*. IEEE, 2015.

[6] G. B. Prince, and T. D. Little, "Latency Constrained Device Positioning Using a Visible Light Communication Two-Phase Received Signal Strength-Angle of Arrival Algorithm." *2015 International Conference on Indoor Positioning and Indoor Navigation (IPIN),* IEEE, 2015, pp:1-7.

[7] H. Kim, D. Kim, S. Yang, Y. Son, and S. Han, "An Indoor Visible Light Communication Positioning System Using a RF Carrier Allocation Technique," *J. Lightw. Technol.*, Vol.31, No.1, 2013, pp. 134-144.

[8] C. Sertthin, T. Ohtsuki, and M. Nakagawa, "6-Axis Sensor Assisted Low Complexity High Accuracy-Visible Light Communication Based Indoor Positioning System," *IEICE Trans. Commun.*, Vol.E93-B, No.11, 2010, pp. 2879-2891.

[9] Y. S. Eroglu, I. Guvenc, N. Pala and M. Yuksel, "AOA-based localization and tracking in multi-element VLC systems," *2015 IEEE 16th Annual Wireless and Microwave Technology Conference (WAMICON)*, Cocoa Beach, FL, 2015, pp. 1-5.

[10] H. Sharifi, A. Kumar, F. Alam and K. M. Arif, "Indoor Localization of Mobile Robot with Visible Light Communication," *2016 12th IEEE/ASME International Conference on Mechatronic and Embedded Systems and Applications (MESA)*, Auckland, 2016, pp. 1-6.

[11] W. Zhang, M. S. Chowdhury, amd M. Kavehrad, "Asynchronous indoor positioning system based on visible light communications." *Optical Engineering*, Vol.53, No.4, 2014, pp.045105.1-045105.9,

[12] A. Sahin, Y.S. Eroglu, I. Guvenc, N. Pala, and M. Yuksel, "Accuracy of AOA-based and RSS-based 3D localization for visible light communications." *Vehicular Technology Conference (VTC Fall)*, 2015 IEEE 82nd. IEEE, 2015.

[13] B. Zhou, V. Lau, Q. Chen, and Y. Cao, "Simultaneous Positioning and Orientating (SPAO) for Visible Light Communications: Algorithm Design and Performance Analysis," *IEEE Transactions on Vehicular Technology*, Vol. 67, No. 12, 2018, PP. 11790-11804

[14] X. Zhang, J. Duan, Y. Fu and A. Shi, "Theoretical Accuracy Analysis of Indoor Visible Light Communication Positioning System Based on Received Signal Strength Indicator," *Journal of Lightwave Technology*, Vol.32, No.21, 2014, pp.4180-4186.

[15] Y. Zhuang, Q. Wang, M. Shi, P. Cao, L. Qi and J. Yang, "Low-Power Centimeter-Level Localization for Indoor Mobile Robots Based on Ensemble Kalman Smoother Using Received Signal Strength," *IEEE Internet of Things Journal*, vol. 6, no. 4, 2019, pp. 6513-6522.

[16] B. Zhou, A. Liu, and V. Lau, "Robust Visible Light-Based Positioning Under Unknown User Device Orientation Angle." *2018 12th International Conference on Signal Processing and Communication Systems (ICSPCS)*. IEEE, 2018.

[17] B. Zhou, A. Liu, and V. Lau, "Joint User Location and Orientation Estimation for Visible Light Communication Systems with Unknown Power Emission," *IEEE Transanctions on Wireless Communications*, 2019

[18] Z. Zhou, M. Kavehrad, and P. Deng, "Indoor Positioning Algorithm using Light-Emitting Diode Visible Light Communications," *Optical Engineering*, 2012, 51(8), 085009-1.

[19] S. H. Yang, H. S. Kim, Y. H. Son and S. K. Han, "Three-Dimensional Visible Light Indoor Localization Using AOA and RSS With Multiple Optical Receivers," *Journal of Lightwave Technology*, Vol.32, No.14, 2014, pp.2480-2485.

[20] Y. Zhuang, L. Hua, L. Qi, J. Yang, P. Cao, Y. Cao, Y. Wu, J. Thompson, and H. Haas, "A Survey of Positioning Systems Using Visible LED Lights," *IEEE Communications Surveys & Tutorials*, Vol.20, No.3, 2018, pp.1963–1988.

[21] B. Zhou, A. Liu, and V. Lau, "Performance Limits of Visible Light-Based User Position and Orientation Estimation Using Received Signal Strength Under NLOS Propagation," *IEEE Transanctions on Wireless Communications*, 2019

[22] C. Amini, A. Taherpour, T. Khattab and S. Gazor, "Theoretical accuracy analysis of indoor visible light communication positioning system based on time-of-arrival," *2016 IEEE Canadian Conference on Electrical and Computer Engineering (CCECE)*, Vancouver, BC, 2016, pp. 1-5.

[23] X. Zhang, J. Duan, Y. Fu and A. Shi, "Theoretical Accuracy Analysis of Indoor Visible Light Communication Positioning System Based on Received Signal Strength Indicator," *Journal of Lightwave Technology*, Vol.32, No.21, 2014, pp.4180-4186.

[24] H. Steendam, T. Q. Wang and J. Armstrong, "Cramer-Rao bound for indoor visible light positioning using an aperture-based angular-diversity receiver," *2016 IEEE Int. Conf. on Communications (ICC)*, Kuala Lumpur, 2016, pp. 1-6.

[25] T. Q. Wang, Y. A. Sekercioglu, A. Neild and J. Armstrong, "Position Accuracy of Time-of-Arrival Based Ranging Using Visible Light With Application in Indoor Localization Systems," *Journal of Lightwave Technology*, Vol.31, No.20, pp.3302-3308, Oct.15, 2013.

[26] A. Al-Kinani, J. Sun, C.-X. Wang, W. Zhang, X. Ge, and H. Haas, "A 2D non-stationary GBSM for vehicular visible light communication channels." *IEEE Transactions on Wireless Communications* (2018).

[27] T. Komine and M. Nakagawa, "Fundamental analysis for visible-light communication system using LED lights," *IEEE Trans. on Consumer Electronics*, Vol.50, No.1, pp.100-107, Feb 2004.

[28] J. H. Y. Nah, R. Parthiban and M. H. Jaward, "Visible Light Communications localization using TDOA-based coherent heterodyne detection," *2013 IEEE 4th International Conference on Photonics (ICP)*, Melaka, 2013, pp. 247-249.

[29] L. Feng, H. Yang, R. Q. Hu, and J. Wang, "mmWave and VLC-Based Indoor Channel Models in 5G Wireless Networks," *IEEE Wireless Communications*, 25.5, (2018): 70-77.

[30] B. Zhou, Q. Chen, P. Xiao and L. Zhao, "On the Spatial Error Propagation Characteristics of Cooperative Localization in Wireless Networks," *IEEE Trans. Vehi. Tech.*, Vol.66, No.2, 2017, pp.1647-1658.

[31] B. Zhou, Q. Chen, and P. Xiao. "The error propagation analysis of the received signal strength-based simultaneous localization and tracking in wireless sensor networks." *IEEE Transactions on Information Theory* 63.6 (2017): 3983-4007.

[32] S. M. Kay, Fundamentals of Statistical Signal Processing, Vol. 2: Detection theory. *Prentice Hall PTR*, 1998.

[33] J. Kahn and J. Barry, “Wireless Infrared Communications,” *Proc. IEEE*, Vol.85, No.2, 1997, pp. 265-298.

[34] M. Yasir, S.-W. Ho, and B. N. Vellambi. ”Indoor positioning system using visible light and accelerometer.” *Journal of Lightwave Technology* 32.19 (2014): 3306-3316.

[35] A. Al-Kinani, C. Wang, H. Haas and Y. Yang, ”A geometry-based multiple bounce model for visible light communication channels.” *Wireless Communications and Mobile Computing Conference (IWCMC), 2016 International*. IEEE, 2016.

[36] A. Sahin, Y. S. Eroglu, I. Guvenc, N. Pala, and M. Yuksel, ”Hybrid 3D Localization for Visible Light Communication Systems”, *IEEE Journal of Lightwave Technology*, vol.33, no.22, 2015, pp.4589-4599.

[37] Y. S. Eroglu, I. Guvenc, A. Sahin, Y. Yapici, N. Pala, and M. Yuksel, ”Multi-Element VLC Networks: LED Assignment, Power Control, and Optimum Combining”, *IEEE Journal on Selected Areas in Communications*, vol. 36, no. 1, 2018, pp. 121-135.

[38] Z. Chen, D. A. Basnayaka, and H. Haas, ”Space division multiple access for optical attocell network using angle diversity transmitters,” *IEEE J. Lightwave Technol.*, vol. 35, no. 11, pp. 2118-2131, 2017

[39] J. Barry, J. Kahn, W. Krause, E. Lee, and D. Messerschmitt, ”Simulation of multipath impulse response for indoor wireless optical channels,” *IEEE J. Select. Areas Commun. (JSAC)*, vol. 11, no. 3, 1993, pp. 367-379.

[40] L. Zeng, D. O’Brien, H. Minh, G. Faulkner, K. Lee, D. Jung, Y. Oh, and E. T. Won, “High Data Rate Multiple Input Multiple Output (MIMO) Optical Wireless Communications Using White LED Lighting,” *IEEE J. Sel. Areas Commun.*, Vol.27, No.9, 2009, pp. 1654-1662.

[41] P. Luo, Z. Ghassemlooy, H. Le Minh, E. Bentley, A. Burton, and X. Tang, ”Fundamental analysis of a car to car visible light communication system.” *Communication Systems, Networks & Digital Signal Processing (CSNDSP), 2014 9th International Symposium on*. IEEE, 2014.

[42] A. Liu, Vincent Lau, and Wei Dai, ”Joint burst LASSO for sparse channel estimation in multi-user massive MIMO.” *2016 IEEE International Conference on Communications (ICC)*. IEEE, 2016.

[43] X. Gao, O. Edfors, F. Rusek, and F. Tufvesson, ”Linear pre-coding performance in measured very-large MIMO channels,” *Proc. IEEE Vehicular Technology Conf. (VTC)*, 2011, pp. 1-5.

[44] C. R. Berger, Z. Wang, J. Huang, and S. Zhou, ”Application of compressive sensing to sparse channel estimation,” *IEEE Commun. Mag.*, vol. 48, no. 11, pp. 164-174, 2010.

[45] W. Bajwa, J. Haupt, A. Sayeed, and R. Nowak, ”Compressed channel sensing: A new approach to estimating sparse multipath channels,” *Proceedings of the IEEE*, vol. 98, no. 6, pp. 1058-1076, June 2010.

[46] Y. Barbotin, A. Hormati, S. Rangan, and M. Vetterli, ”Estimation of sparse MIMO channels with common support,” *IEEE Trans. Commun.*, vol. 60, no. 12, pp. 3705-3716, Dec. 2012.

[47] D. Tse and P. Viswanath, ”*Fundamentals of wireless communication*.” Cambridge Univ Pr, 2005.

[48] J. Poutanen, K. Haneda, J. Salmi, V. Kolmonen, F. Tufvesson, T. Hult, and P. Vainikainen, ”Significance of common scatterers in multi-link indoor radio wave propagation,” *Proc. IEEE European Conf. Antennas and Propagation (EuCAP)*, 2010, pp. 1-5